International Journal on Advances in Networks and Services

2022 vol. 15 nr. 3&4

The *International Journal on Advances in Networks and Services* is published by IARIA.
ISSN: 1942-2644
journals site: http://www.iariajournals.org
contact: petre@iaria.org

Sponsored by IARIA
www.iaria.org

International Journal on Advances in Networks and Services
Volume 15, Number 3 & 4, 2022

Maria-Dolores Cano, Universidad Politécnica de Cartagena, Spain
Juan-Vicente Capella-Hernández, Universitat Politècnica de València, Spain
Eduardo Cerqueira, Federal University of Para, Brazil
Bruno Chatras, Orange Labs, France
Marc Cheboldaeff, Deloitte Consulting GmbH, Germany
Kong Cheng, Vencore Labs, USA
Dickson Chiu, Dickson Computer Systems, Hong Kong
Andrzej Chydzinski, Silesian University of Technology, Poland
Hugo Coll Ferri, Polytechnic University of Valencia, Spain
Noelia Correia, University of the Algarve, Portugal
Noël Crespi, Institut Telecom, Telecom SudParis, France
Paulo da Fonseca Pinto, Universidade Nova de Lisboa, Portugal
Orhan Dagdeviren, International Computer Institute/Ege University, Turkey
Philip Davies, Bournemouth and Poole College / Bournemouth University, UK
Carlton Davis, École Polytechnique de Montréal, Canada
Claudio de Castro Monteiro, Federal Institute of Education, Science and Technology of Tocantins, Brazil
João Henrique de Souza Pereira, University of São Paulo, Brazil
Javier Del Ser, Tecnalia Research & Innovation, Spain
Behnam Dezfouli, Universiti Teknologi Malaysia (UTM), Malaysia
Daniela Dragomirescu, LAAS-CNRS, University of Toulouse, France
Jean-Michel Dricot, Université Libre de Bruxelles, Belgium
Wan Du, Nanyang Technological University (NTU), Singapore
Matthias Ehmann, Universität Bayreuth, Germany
Wael M El-Medany, University Of Bahrain, Bahrain
Imad H. Elhajj, American University of Beirut, Lebanon
Gledson Elias, Federal University of Paraíba, Brazil
Rainer Falk, Siemens AG - Corporate Technology, Germany
Károly Farkas, Budapest University of Technology and Economics, Hungary
Huei-Wen Ferng, National Taiwan University of Science and Technology - Taipei, Taiwan
Gianluigi Ferrari, University of Parma, Italy
Mário F. S. Ferreira, University of Aveiro, Portugal
Bruno Filipe Marques, Polytechnic Institute of Viseu, Portugal
Ulrich Flegel, HFT Stuttgart, Germany
Juan J. Flores, Universidad Michoacana, Mexico
Ingo Friese, Deutsche Telekom AG - Berlin, Germany
Sebastian Fudickar, University of Potsdam, Germany
Stefania Galizia, Innova S.p.A., Italy
Ivan Ganchev, University of Limerick, Ireland / University of Plovdiv “Paisii Hilendarski”, Bulgaria
Miguel Garcia, Universitat Politecnica de Valencia, Spain
Emiliano Garcia-Palacios, Queens University Belfast, UK
Marc Gilg, University of Haute-Alsace, France
Debasis Giri, Haldia Institute of Technology, India
Markus Goldstein, Kyushu University, Japan
Luis Gomes, Universidade Nova Lisboa, Portugal
Anahita Gouya, Solution Architect, France
Mohamed Graiet, Institut Supérieur d'Informatique et de Mathématique de Monastir, Tunisie
Christos Grecos, University of West of Scotland, UK
Vic Grout, Glyndwr University, UK
Yi Gu, Middle Tennessee State University, USA
Angela Guercio, Kent State University, USA
Xiang Gui, Massey University, New Zealand
Mina S. Guirguis, Texas State University - San Marcos, USA
Tibor Gyires, School of Information Technology, Illinois State University, USA

Keijo Haataja, University of Eastern Finland, Finland
Gerhard Hancke, Royal Holloway / University of London, UK
R. Hariprakash, Arulmigu Meenakshi Amman College of Engineering, Chennai, India
Eva Hladká, CESNET & Masaryk University, Czech Republic
Hans-Joachim Hof, Munich University of Applied Sciences, Germany
Razib Iqbal, Amdocs, Canada
Abhaya Induruwa, Canterbury Christ Church University, UK
Muhammad Ismail, University of Waterloo, Canada
Vasanth Iyer, Florida International University, Miami, USA
Imad Jawhar, United Arab Emirates University, UAE
Aravind Kailas, University of North Carolina at Charlotte, USA
Mohamed Abd rabou Ahmed Kalil, Ilmenau University of Technology, Germany
Kyoung-Don Kang, State University of New York at Binghamton, USA
Sarfraz Khokhar, Cisco Systems Inc., USA
Vitaly Klyuev, University of Aizu, Japan
Jarkko Kneckt, Nokia Research Center, Finland
Dan Komosny, Brno University of Technology, Czech Republic
Ilker Korkmaz, Izmir University of Economics, Turkey
Tomas Koutny, University of West Bohemia, Czech Republic
Evangelos Kranakis, Carleton University - Ottawa, Canada
Lars Krueger, T-Systems International GmbH, Germany
Kae Hsiang Kwong, MIMOS Berhad, Malaysia
KP Lam, University of Keele, UK
Birger Lantow, University of Rostock, Germany
Hadi Larijani, Glasgow Caledonian Univ., UK
Annett Laube-Rosenpflanzer, Bern University of Applied Sciences, Switzerland
Gyu Myoung Lee, Institut Telecom, Telecom SudParis, France
Shiguo Lian, Orange Labs Beijing, China
Chiu-Kuo Liang, Chung Hua University, Hsinchu, Taiwan
Wei-Ming Lin, University of Texas at San Antonio, USA
David Lizcano, Universidad a Distancia de Madrid, Spain
Chengnian Long, Shanghai Jiao Tong University, China
Jonathan Loo, Middlesex University, UK
Pascal Lorenz, University of Haute Alsace, France
Albert A. Lysko, Council for Scientific and Industrial Research (CSIR), South Africa
Pavel Mach, Czech Technical University in Prague, Czech Republic
Elsa María Macías López, University of Las Palmas de Gran Canaria, Spain
Damien Magoni, University of Bordeaux, France
Ahmed Mahdy, Texas A&M University-Corpus Christi, USA
Zoubir Mammeri, IRIT - Paul Sabatier University - Toulouse, France
Gianfranco Manes, University of Florence, Italy
Sathiamoorthy Manoharan, University of Auckland, New Zealand
Moshe Timothy Masonta, Council for Scientific and Industrial Research (CSIR), Pretoria, South Africa
Hamid Menouar, QU Wireless Innovations Center - Doha, Qatar
Guowang Miao, KTH, The Royal Institute of Technology, Sweden
Mohssen Mohammed, University of Cape Town, South Africa
Miklos Molnar, University Montpellier 2, France
Lorenzo Mossucca, Istituto Superiore Mario Boella, Italy
Jogesh K. Muppala, The Hong Kong University of Science and Technology, Hong Kong
Katsuhiro Naito, Mie University, Japan
Deok Hee Nam, Wilberforce University, USA
Sarmistha Neogy, Jadavpur University- Kolkata, India
Rui Neto Marinheiro, Instituto Universitário de Lisboa (ISCTE-IUL), Instituto de Telecomunicações, Portugal

David Newell, Bournemouth University - Bournemouth, UK
Ngoc Tu Nguyen, Missouri University of Science and Technology - Rolla, USA
Armando Nolasco Pinto, Universidade de Aveiro / Instituto de Telecomunicações, Portugal
Jason R.C. Nurse, University of Oxford, UK
Kazuya Odagiri, Sugiyama Jyogakuen University, Japan
Máirtín O'Droma, University of Limerick, Ireland
Jose Oscar Fajardo, University of the Basque Country, Spain
Constantin Paleologu, University Politehnica of Bucharest, Romania
Eleni Patouni, National & Kapodistrian University of Athens, Greece
Harry Perros, NC State University, USA
Miodrag Potkonjak, University of California - Los Angeles, USA
Yusnita Rahayu, Universiti Malaysia Pahang (UMP), Malaysia
Yenumula B. Reddy, Grambling State University, USA
Oliviero Riganelli, University of Milano Bicocca, Italy
Antonio Ruiz Martinez, University of Murcia, Spain
George S. Oreku, TIRDO / North West University, Tanzania/ South Africa
Sattar B. Sadkhan, Chairman of IEEE IRAQ Section, Iraq
Husnain Saeed, National University of Sciences & Technology (NUST), Pakistan
Addisson Salazar, Universidad Politecnica de Valencia, Spain
Sébastien Salva, University of Auvergne, France
Ioakeim Samaras, Aristotle University of Thessaloniki, Greece
Luz A. Sánchez-Gálvez, Benemérita Universidad Autónoma de Puebla, México
Teerapat Sanguankotchakorn, Asian Institute of Technology, Thailand
José Santa, University Centre of Defence at the Spanish Air Force Academy, Spain
Rajarshi Sanyal, Belgacom International Carrier Services, Belgium
Mohamad Sayed Hassan, Orange Labs, France
Thomas C. Schmidt, HAW Hamburg, Germany
Véronique Sebastien, University of Reunion Island, France
Jean-Pierre Seifert, Technische Universität Berlin & Telekom Innovation Laboratories, Germany
Dimitrios Serpanos, Univ. of Patras and ISI/RC ATHENA, Greece
Roman Y. Shtykh, Rakuten, Inc., Japan
Salman Ijaz Institute of Systems and Robotics, University of Algarve, Portugal
Adão Silva, University of Aveiro / Institute of Telecommunications, Portugal
Florian Skopik, AIT Austrian Institute of Technology, Austria
Karel Slavicek, Masaryk University, Czech Republic
Vahid Solouk, Urmia University of Technology, Iran
Peter Soreanu, ORT Braude College, Israel
Pedro Sousa, University of Minho, Portugal
Cristian Stanciu, University Politehnica of Bucharest, Romania
Vladimir Stantchev, SRH University Berlin, Germany
Radu Stoleru, Texas A&M University - College Station, USA
Lars Strand, Nofas, Norway
Stefan Strauβ, Austrian Academy of Sciences, Austria
Álvaro Suárez Sarmiento, University of Las Palmas de Gran Canaria, Spain
Masashi Sugano, School of Knowledge and Information Systems, Osaka Prefecture University, Japan
Young-Joo Suh, POSTECH (Pohang University of Science and Technology), Korea
Junzhao Sun, University of Oulu, Finland
David R. Surma, Indiana University South Bend, USA
Yongning Tang, School of Information Technology, Illinois State University, USA
Yoshiaki Taniguchi, Kindai University, Japan
Anel Tanovic, BH Telecom d.d. Sarajevo, Bosnia and Herzegovina
Rui Teng, Advanced Telecommunications Research Institute International, Japan
Olivier Terzo, Istituto Superiore Mario Boella - Torino, Italy

International Journal on Advances in Networks and Services
Volume 15, Numbers 3 & 4, 2022

CONTENTS

A System for Indoor Guidance Using Visible Light Communication

Manuela Vieira, Manuel Augusto Vieira, Paula Louro, Alessandro Fantoni
ADETC/ISEL/IPL,
R. Conselheiro Emídio Navarro, 1959-007
Lisboa, Portugal
CTS-UNINOVA
Quinta da Torre, Monte da Caparica, 2829-516,
Caparica, Portugal

e-mail: mv@isel.ipl.pt, mv@isel.pt, plouro@deetc.isel.pt, afantoni@deetc.isel.ipl.pt

Pedro Vieira
ADETC/ISEL/IPL,
R. Conselheiro Emídio Navarro, 1959-007
Lisboa, Portugal
Instituto das Telecomunicações
Instituto Superior Técnico, 1049-001,
Lisboa, Portugal
e-mail: pvieira@isel.pt

***Abstract*— Communications within personal working/living spaces are highly demanded. To support people's wayfinding activities, we propose a Visible Light Communication (VLC) cooperative system that supports guidance services and uses an edge/fog-based architecture for wayfinding services. A mesh cellular hybrid structure is proposed. The dynamic navigation system is composed of several transmitters (ceiling luminaries), which send the map information and path messages required to wayfinding. The luminaires are equipped with one of two types of nodes: a "mesh" controller that connects with other nodes in its vicinity and can forward messages to other devices in the mesh, effectively acting like routers nodes in the network and a "mesh/cellular" hybrid controller, that is also equipped with a modem providing IP base connectivity to the central manager services. These nodes act as border-router and can be used for edge computing. Mobile optical receivers, using joint transmission, collect the data at high frame rates, extracts their location to perform positioning and, concomitantly, the transmitted data from each transmitter. Each luminaire, through VLC, reports its geographic position and specific information to the users, making it available for whatever use. Bidirectional communication is implemented and the best route to navigate through venue calculated. The results show that the system makes possible not only the self-localization, but also to infer the travel direction and to interact with information received optimizing the route towards a static or dynamic destination.**

Keywords- Visible Light Communication; Indoor navigation; Bidirectional Communication; Wayfinding; Optical sensors; Indoor multi-level environments; Transmitter/Receiver.

I. INTRODUCTION

This paper is an extended version from the one presented in ALLSENSORS 2022 [1].

Nowadays, wireless networks have seen a demand for increased data rate requirements. For a realistic coverage with the data rate requirements, a large bandwidth is needed which remains a limiting factor when compared with the RF communication technologies. Consequently, research has started exploring alternate wireless transmission technologies to meet the ever-increasing demand. In this context, the huge bandwidth available in the unlicensed electromagnetic spectrum in the optical domain is seen as a promising solution to the spectrum crunch.

Visible Light Communication (VLC) makes use of the higher frequencies in the visual band and extends the capabilities of data transmission using general light sources. VLC has been regarded as an additional communication technology [2] [3] to fulfill the high data rate demands and as a new affiliate in the beyond fifth generation (5G) heterogeneous networks. It can be easily used in indoor environments using the existing LED lighting infrastructure with few modifications [4] [5]. Research has shown that compared to outdoors, people tend to lose orientation a lot easier within complex buildings [6] [7]. Fine-grained indoor localization can be useful, enabling several applications [8] [9].

This work focuses on the use of VLC as a support for the transmission of information, providing advertising services and specific information to users. The goal is a cooperative system that supports guidance services and uses an edge/fog based architecture for wayfinding services. Here, the luminaire, through VLC, reports its geographical positions and specific information to the users since its infrastructure can also be reused to embed the fog nodes in them. The system is composed of several transmitters (LEDs luminaries), which send the map information and path messages required to wayfinding. Data is encoded, modulated and converted into light signals emitted by the transmitters. Every mobile terminal is equipped with a receiver module for receiving the mapped information generated from the ceiling light and displays this information in the mobile terminal. The receiver module includes a photodetector based on a tandem a-SiC:H/a-Si:H pin/pin light-controlled filter [10] [11].

Visible light can be used as an ID system and can be employed for identifying the room number and the building itself. The main idea is to divide the service area into spatial

beams originating from the different ID light sources and identify each beam with a unique timed sequence of light signals. The signboards, based on arrays of LEDs, positioned in strategic directions to broadcast the information [12], are modulated acting as down- and up-link channels in the bidirectional communication. For the consumer services, the applications are enormous. The objective is to allow the implementation of new services in these areas using data from the VLC System, for indoor and outdoor. Positioning, navigation, security and even mission critical services are possible use cases that should be implemented.

In this paper, a LED-supported guidance VLC system is proposed. After the Introduction, in Section II, the communication system is described. In Section III, the main experimental results are presented, downlink and uplink transmission is implemented and the best route to navigate calculated. In Section IV, the conclusions are drawn.

II. COMMUNICATION SYSTEM, DESIGN AND ARCHITECTURE

The main goal is to specify the system conceptual design and define a set of use cases for a VLC based guidance system to be used by mobile users inside large buildings.

A. *Communication system and cooperative localization*

The system is composed by two modules: the transmitter and the receiver.

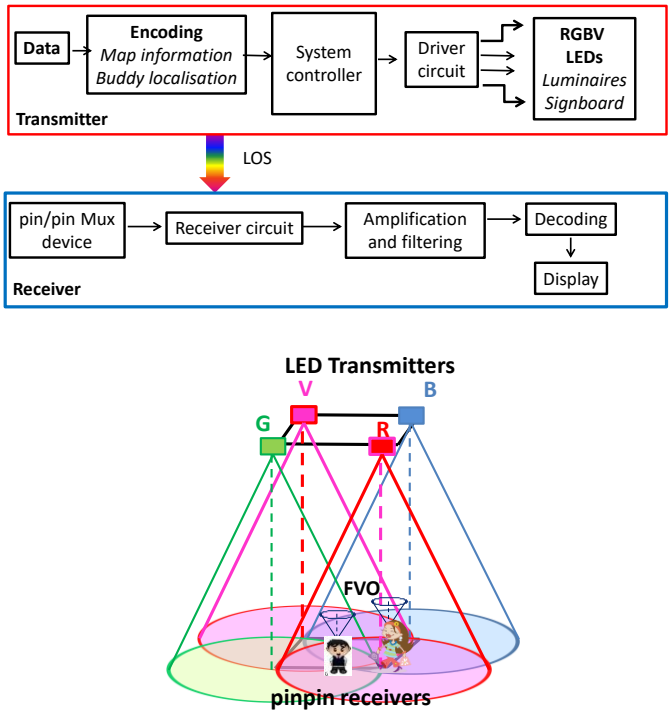

Figure 1. Block diagram and transmitters and receivers 3D relative positions.

The block diagram and the transmitter and receiver relative positions are presented in Figure 1. Both communication modules are software defined, where modulation/ demodulation can be programed.

Data from the sender is converted into an intermediate data representation, byte format, and converted into light signals emitted by the transmitter module. The data bit stream is input to a modulator where an ON–OFF Keying (OOK) modulation is utilized. On the transmission side, a modulation and conversion from digital to analog data is done. The driver circuit will keep an average value (DC power level) for illumination, combining it with the analog data intended for communication. The visible light emitted by the LEDs passes through the transmission medium and is then received by the MUX device.

To realize both the communication and the building illumination, white light tetra-chromatic sources are used providing a different data channel for each chip. Each luminaire is composed of four white LEDs framed at the corners of a square (Figure 2). At each node, only one chip of the LED is modulated for data transmission, the Red (R: 626 nm), the Green (G: 530 nm), the Blue (B: 470 nm) or the Violet (V). In Figure 2a, the spectra of the input channels is displayed.

Data is encoded, modulated and converted into light signals emitted by the transmitters. Modulation and digital-to-analog conversion of the information bits is done using signal processing techniques.

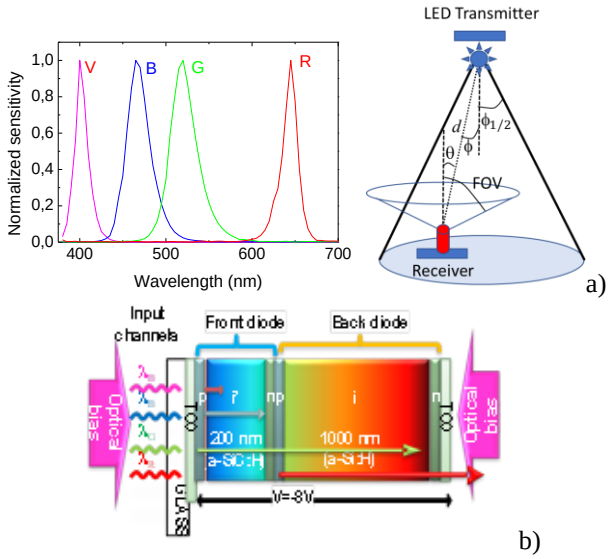

Figure 2. a) Spectra of the input channels. b) Configuration and operation of the pin/pin Mux device.

The signal is propagating through the optical channel, and a VLC receiver, at the reception end of the communication link, is responsible to extract the data from the modulated light beam. It transforms the light signal into an electrical signal that is subsequently decoded to extract the transmitted information. The obtained voltage is then

processed, by using signal conditioning techniques (adaptive bandpass filtering and amplification, triggering and demultiplexing), until the data signal is reconstructed at the data processing unit (digital conversion, decoding and decision) [13] [14]. At last, the message will be output to the users.

In the receiving system, a MUX photodetector acts as an active filter for the visible spectrum. The VLC photosensitive receiver is a double pin/pin photodetector based on a tandem heterostructure, p-i'-n/p-i-n sandwiched between two conductive transparent contacts (Figure 2a). The front, thin pi'n structure made of a-SiC:H exhibits high absorption to short wavelengths (violet and blue light) and high transparency to the long wavelength (red light). In opposition, the back, thicker pin structure based on a-Si:H absorbs long wavelengths (red light), the green light is absorbed in both structures. The device selectivity is tuned externally using reverse bias (-8 V) and optical steady state illumination of short wavelength (400 nm). Exposed to light, the device offers high sensitivity and linear response, generating a proportional electrical current. Its quick response enables the possibility of high-speed communications. Since the photodetector response is insensitive to the frequency, phase, or polarization of the carriers, this kind of receiver is useful for intensity-modulated signals. The generated photocurrent is processed using a transimpedance circuit obtaining a proportional voltage. Since the photodetector response is insensitive to the frequency, phase, or polarization of the carriers, this kind of receiver is useful for intensity-modulated signals. After receiving the signal, it is in turn filtered, amplified, and converted back to digital format for demodulation. The system controller consists of a set of programmable modules.

In this system model, there are a few assumptions that should be noted: the channel state information is available both at the receiver and the transmitter; compared with the direct light, the reflected light is much weaker in the indoor VLC systems; only the Line OF Sight (LOS) path is considered and the multipath influence is not considered in the proposed indoor VLC system.

The received channel can be expresssed as:

$$y=\mu hx+n \quad (1)$$

where y represents the received signal, x the transmitted signal, μ is the photoelectric conversion factor which can be normalized as $\mu = 1$, h is the channel gain and n is the additive white Gaussian noise of which the mean is 0.

The LEDs are modeled as Lambertian sources where the luminance is distributed uniformly in all directions, whereas the luminous intensity is different in all directions. The luminous intensity for a Lambertian source is given by Eq. (2) [15]:

$$I(\emptyset) = I_N \cos(\emptyset)^m \quad ; \quad m = \frac{\ln(2)}{\ln(\cos(\phi_{1/2}))} \quad (2)$$

I_N is the maximum luminous intensity in the axial direction, ϕ is the angle of irradiance and m is the order derived from a Lambertian pattern. For the proposed system, the commercial white LEDs were designed for illumination purposes, exhibiting a wide half intensity angle ($\phi_{1/2}$) of 60º. Thus, the Lambertian order m is 1. Friis' transmission equation is frequently used to calculate the maximum range by which a wireless link can operate. The coverage map is obtained by calculating the link budget from the Friis Transmission Equation [16]. The Friis transmission equation relates the received power (P_R) to the transmitted power (P_E), path loss distance (L_R), and gains from the emitter (G_E) and receiver (G_R) in a free-space communication link.

$$P_R\,[dBm] = P_E\,[dBm] + G_E\,[dB] + G_R\,[dB] - L_R\,[dB] \quad (3)$$

Taking into account Figure 2a, the path loss distance and the emitter gain will be given by:

$$L_R\,[dB] = 22 + 20\ln\frac{d}{\lambda} \quad (4)$$

$$G_E\,[dB] = \frac{(m+1)A}{2\pi d_{E-R}^2} I(\emptyset)\cos(\theta) \quad (5)$$

With A de area of the photodetector and d_{E_R} the distance between each transmitter and every point on the receiver plane. Due to their filtering properties of the receptors the gains are strongly dependent on the wavelength of the pulsed LEDs. Gains (G_R) of 5, 4, 1.7 and 0.8 were used, respectively, for the R, G, B and V LEDs. I_N of 730 mcd, 650 mcd, 800 mcd and 900 mcd were considered.

Taking into account Equations (1)-(5), the coverage map for a square unit cell is displayed in Figure 3a. All the values were converted to decibel (dB).

On the receiving side, this is first done by a silicon carbide (SiC) pinpin MUX device that acts as an active filter for the visible region of the light spectrum. After receiving the signal, it is in turn filtered, amplified, and converted back to digital format for demodulation. The system controller consists of a set of programmable modules. To receive the I2V information from several transmitters, the receiver must be located at the overlap of the circles that set the transmission range (radial) of each transmitter. The coverage map for a square unit cell is displayed in Figure 3. The LEDs are modeled as Lambertian sources where the luminance is distributed uniformly in all directions, whereas the luminous intensity is different in all directions [15]. The nine possible overlaps (#1-#9), defined as fingerprint regions, as well as receiver orientations (2-9 steering angles; δ) are also pointed out for the unit square cell in Figure 3a.

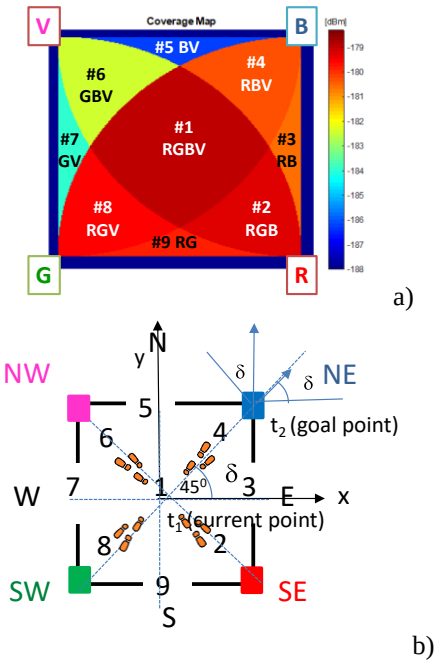

Figure 3. Illustration of: a) the coverage map in the unit cell. b) Footprint regions (#1-#9) and steering angle codes (2-9).

The input of the aided navigation system is the coded signal sent by the transmitters to an identify user, and includes its position in the network *P(x, y, z)*, inside the unit cell and the steering angle, δ, that guides the user across his path. The device receives multiple signals, finds the centroid of the received coordinates, and stores it as the reference point position. Nine reference points, for each unit cell, are identified giving a fine-grained resolution in the localization of the mobile device across each cell.

Along with the robustness of the electronic devices used, modulation is also paramount to ensure the VLC systems' performance and commercial viability. The core difference between VLC and regular RF (Radio-Frequency) communications is that VLC does not allow for amplitude and phase modulation techniques and must encode information by varying the intensity of emitted light.

An OOK modulation scheme was used to code the information. In OOK, the data bits are transmitted by having the LED illuminating at different intensity levels. For example, having the LED at its maximum brightness ("on") when transmitting the data bit '1' and dimmed ("off") when transmitting the data bit '0', this way digital data is represented by the presence or absence of a carrier wave. The main advantage of OOK is its simplicity and subsequent ease of implementation, whereas its main limiting factor are low data rates further exacerbated in systems using different dimming levels.

The obtained voltage is then processed, by using signal conditioning techniques (adaptive bandpass filtering and amplification, triggering and demultiplexing), until the data signal is reconstructed at the data processing unit (digital conversion, decoding and decision) [14].

B. Architecture and Multi-person Cooperative Localization

Fog/Edge computing bridges the gap between the cloud and end devices by enabling computing, storage, networking, and data management on network nodes within the close vicinity of IoT devices. Fog computing has advantages since it provides moderate availability of computing resources at lower power consumption. Computing resources may be used for caching at the edge of the network, which enables faster retrieval of content and a lower burden on the front-haul. The edge is the immediate first hop from the IoT devices, such as the LiFi access points or gateways. In edge computing, the computation is done at the edge of the network through small data centers that are close to users. A mesh network is a good fit since it dynamically reconfigures itself and grows with the size of any installation. In Figure 4, the proposed architecture is illustrated.

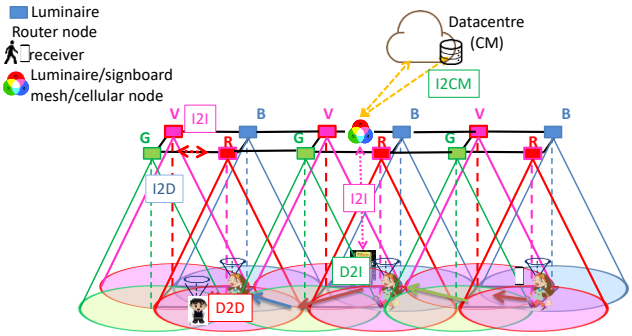

Figure 4. Mesh and cellular hybrid architecture.

The luminaires are equipped with one of two types of controllers: A "mesh" controller that connects with other nodes in its vicinity and can forward messages to other devices (I2D) in the mesh, effectively acting like routers nodes in the network. A "mesh/cellular" hybrid controller, that is also equipped with a modem providing IP base connectivity to the central manager services (I2CM). These nodes act as border-routers and can be used for edge computing. So, edge computing is located at the edge of the network close to end-user devices.

Under this architecture, the short-range mesh network purpose is twofold: enable edge computing and device-to-cloud communication, by ensuring a secure communication from a luminaire controller to the edge computer or datacenter (I2CM), through a neighbor luminaire/signboard controller with an active cellular connection; and enable peer-to-peer communication (I2I), to exchange information. It performs much of the processing on embedded computing platforms, directly interfacing to sensors and controllers. It

supports geo-distribution, local decision making, and real-time load-balancing. Moreover, it depends on the collaboration of near-located end-user devices, instead of relying on the remote servers, which reduces the deployment costs and delay.

C. Self-localization

Self-localization is a fundamental issue since the person must be able to estimate its position and orientation (pose) within a map of the environment it is navigating. We consider the path to be a geometric representation of a plan to move from a start pose to a goal pose (Figure 2). Let us consider a person navigating in a 2D environment. Its non-omnidirectional configuration is defined by position (x, y) and orientation angle δ, with respect to the coordinate axes. q(t) = [*x(t), y(t), δ(t)*] denote its pose at time *t*, in a global reference frame. In cooperative positioning systems, persons are divided into two groups, the stationary persons and the moving persons. Let us consider that $q_i(t,t')$ represents the pose of person *i* at time *t´* relative to the pose of the same person at time *t* and $q_{ij}(t)$ denotes the pose of person *j* relative to the pose of person *i* at time *t*. $q_i(t,t')$ is null for people standing still and non-zero if they move. These three types of information $q_i(t)$, $q_i(t,t')$and $q_{ij}(t)$ compose the basic elements of a pose graph for multi-person cooperative localization.

We consider that the risk of virus transmission exists if $q_{ij}(t)$ is less than 2 m. The system will alert the users to stay away from those regions and to plan the better route to the desired wayfinding services. To estimate each person track the pure pursuit approach [17], [18] is used. The principle takes into account the curvature required for the mobile receiver to steer from its current position (t_1) to its intended position (t_2). By specifying a look-ahead distance, it defines the radius of an imaginary circle. Finally, a control algorithm chooses a steering angle in relation to this circle. This then allows to iteratively construct the intermediate arcs between itself and its goal position as it moved, thus, obtaining the required trajectory for it to reach its objective position. To avoid the risk of transmission, in the same frame of time and in known crowded regions, $q_{ij}(t)$ is estimated and the steering angle readjusted [19].

D. Scenario and building model

A navigation system refers to one that can identify the geographical coordinates of a user or device through a variety of data collecting mechanisms such as network routing addresses or geolocation devices. Once obtained, these coordinates determine the location of the user and allow them to "navigate" the map of an unfamiliar area by informing them of where they are, where their destination is, and step-by-step directions on what is the best route to get there. When it comes to outdoor positioning, the GPS (Global Positioning System) has been the most common means of identifying a user's location, such as when driving a vehicle. But when it comes to indoor navigation it is still far from maturity. The GPS cannot be relied on for this since satellite signals have trouble penetrating most buildings' rooves, tunnels, or floors.

When utilizing a navigation system, users wish to be guided on a direct, shortest path, to their destination based on their current position (starting point) and where they wish to go (destination point). For this purpose, VLC utilizes cells for positioning along with a CM (Central Manager) to keep track of everything and generate the optimal path.

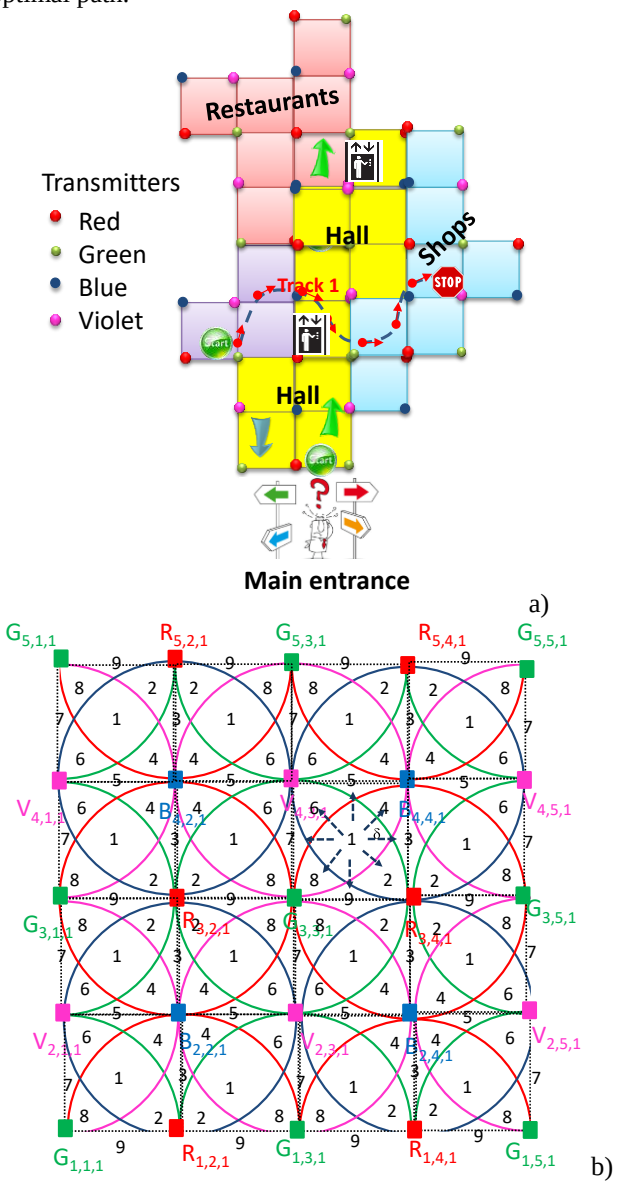

Figure 5. a) proposed scenario. b) Illustration of the 2D optical scenario (RGBV =modulated LEDs spots). Clusters of cells in square topology.

In VLC geotracking, geographic coordinates are generated, but the feature's usefulness is enhanced by using them to determine a meaningful location, to guide the user through an unfamiliar building, or to lead him to his desired

meeting destination. It is believed this type of indoor location service would be most impactful in large-sized buildings with many points of interest and daily visitors, such as shopping malls and airports.

Building a geometry model of buildings' interiors is complex. Indoor VLC cell design is especially important since, being man-made, buildings such as these commonly follow basic shapes (squares, equilateral triangles/regular hexagons). In the proposed architecture each room/crossing/exit represents a node, and a path as the links between nodes. The proposed scenario is a multi-level building (Figure 5a). Lighting in large environments is designed to illuminate the entire space in a uniform way. Ceiling plans for the LED array layout, in floor level is shown in Figure 5b. A square lattice topology was considered for each level. A user navigates from outdoor to indoor. This topology is represented using *x*, *y* and *z* axes to simplify both the figure comprehension and the distance between any pair of nodes. In Figure 6 the 3D building model is depicted.

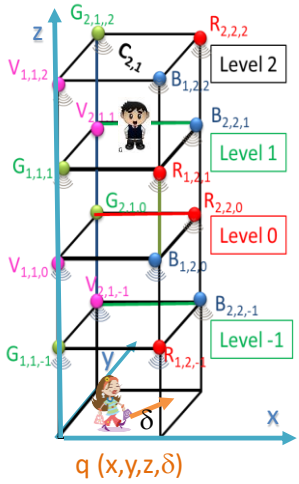

Figure 6. Illustration of the 3D optical scenario (RGBV =modulated LEDs spots). Row of cells in square topology.

Each node emits light all around it and up to a certain range, which allows each cell to be divided into footprints depending on which LEDs are covering any given space (Figure 3a), thus allowing the system to determine the position of a user or device in any given cell, q(x,y,z,δ).

A generated path to the end point can be viewed as a sequence of directions to nearby checkpoints that require the user to change their direction or steering angle (turning a corner, going around something, etc.). This means that a navigation system must also be able to identify the angle the user is moving in and the angle between the user and the next checkpoint (Figure 3b).

The user sends a request message to find the right track (D2I, in Figure 4) and, in the available time, he adds customized points of interest (wayfinding services). The requested information (I2D) is sent by the emitters at the ceiling to its receiver. The indoor route throughout the building (track) is presented to the user by a responding message transmitted by the ceiling luminaires that work also either as router or mesh/cellular nodes. With this request/response concept, the generated landmark-based instructions help the user to unambiguously identify the correct decision point where a change of direction (pose) is needed, as well as offer information for the user to confirm that he/she is on the right way.

III. GEOTRACKING, NAVIGATION AND ROUTE CONTROL

Bi-directional communication between the infrastructure and the mobile receiver is analyzed.

A. Communication protocol and coding/decoding techniques

In order to ensure a synchronized and organized link between the user device and the various emitters, the use of a communication protocol for both encoding and decoding the shared data is important. To achieve this communication protocol, packets of bits are used, referred to as data frames, where its contents are formed from the required navigation data and arranged into several fields.

To code the information, an On-Off Keying (OOK) modulation scheme was used, and it was considered a synchronous transmission based on a 64- bits data frame.

Table 1. Frame structure

Header	**Navigation Data**						**Payload**	
Synch	x	y	z	pin_1	pin_2	δ	Wayfinding data	Stop bit
5 bits (10101)	24 bits (4 bits per field)						34 bits (0 0)	1 bit (0)
Frame length = 64 bits								

The frame is divided into three main blocks (Sync, Navigation data and Payload). The header block is the synchronization block [10101] This first block is named the header and refers to the starting bit sequence that is repeated in every data frame and allows the receiver to determine from an array of incoming bits where each frame begins. For this purpose, the same header bit sequence is imposed simultaneously to all emitters, in this case in an alternating "on"- "off" pattern [10101]. The second block contains the ID, 4+4+4 bits, gives the geolocation (*x*,*y*,*z* coordinates) of the emitters inside the array ($X_{i,j,k}$). These IDs were encoded using a 4-bit binary representation for the decimal number. The z coordinate refers to the floor number, which can be negative (ex: garages, machine rooms, warehouses, etc.) and is much less likely to reach double-digit values (skyscrapers being the most glaring exception); thus the first bit is used to represent the floor number's sign ('0' when a positive number, '1' when a negative number) and the remaining three bits indicating the coordinate's value.

When bidirectional communication is required, the user must register by choosing a username (pin_1) with 4 decimal numbers, each one associated to a RGBV channel. If buddy friend services are required a 4-binary code of the meeting (pin_2) must be inserted. The δ block (steering angle (δ)), a 4-bit sequence, completes the user's pose in a frame time q(x,y, δ, t). Eight steering angles along the cardinal points are possible from a start point to the next goal as pointed out as dotted arrows in Figure 5. The codes assigned to the pin_2 and to δ are the same in all the channels. If no wayfinding services are required these last three blocks are set at zero and the user only receives its own location.

The third and final block is named the payload and refers to sequence of bits that is not necessary for the navigation service. It is made up of miscellaneous data and followed by a stop bit. The frame payload starts with a sequence of bits that, while unnecessary for navigation, can be used to add more functionality to the indoor navigation service or even be used to improve the already existing one. The inclusion of a messaging service between users or a resending of one or more fields, are only two examples of how the payload can be used in a large-scale application.

Based on the measured photocurrent signal by the photodetector, it is necessary to decode the information received. A calibration curve is previously defined to establish this assignment. In Figure 7a, it is plotted the calibration curve that uses 16 distinct photocurrent thresholds resultant from the combination of the RGBV modulated signals from VLC emitter. The correspondence between each 4-binary code and the photocurrent level is highlighted on the right side. Here, the MUX signal obtained at the receiver as well as the coded transmitted optical signals is displayed. The message, in the frame, starts with the header labelled as Sync, a block of 5 bits. The same synchronization header [10101] is imposed simultaneously to all emitters. In the second block, labelled as calibration, the bit sequence was chosen to allow all the *on/off* sixteen possible combinations of the four RGBV input channels (2^4). Finally, a random message was transmitted [20]. Comparing the calibrated levels (d_0-d_{15}) with the different assigned 4-digit binary [RGBV] codes, ascribed to each level, the decoding is straightforward, and the message decoded [21].

In Figure 7b, the MUX received signal and the decoding information that allows the VLC geotracking and guidance in successive instants (t_0, t_1, t_2) from user "7261" guiding him along his track is exemplified. The visualized cells, paths, and the reference points (footprints) are also shown as inserts. Data shows that at t_0 the network location of the received signals is $R_{3,2,1}$, $G_{3,1,1}$, $B_{4,2,1}$ and $V_{4,1,1}$, at t_1 the user receives the signal only from the $R_{3,2,1}$, $B_{4,2,1}$ nodes and at t_2 he was moved to the next cell since the node $G_{3,1,1}$ was added at the receiver. Hence, the mobile user "7261" begins his route into position #1 (t_0) and wants to be directed to his goal position, in the next cell (# 9). During the route the navigator is guided to E (code 3) and, at t_1, steers to SE (code 2), cross footprint #2 (t_3) and arrives to #9. The ceiling lamps (landmarks) spread over all the building and act as edge/fog nodes in the network, providing well-structured paths that maintain a navigator's orientation with respect to both the next landmark along the path and the distance to the eventual destination. Also, the VLC dynamic system enables cooperative and oppositional geolocation. In some cases, it is in the user's interest to be accurately located, so that they can be offered information relevant to their location and orientation (pin_1, pin_2 and δ blocks). In other cases, users prefer not to disclose their location for privacy, in this case these last three blocks are set at zero and the user only receives its own location.

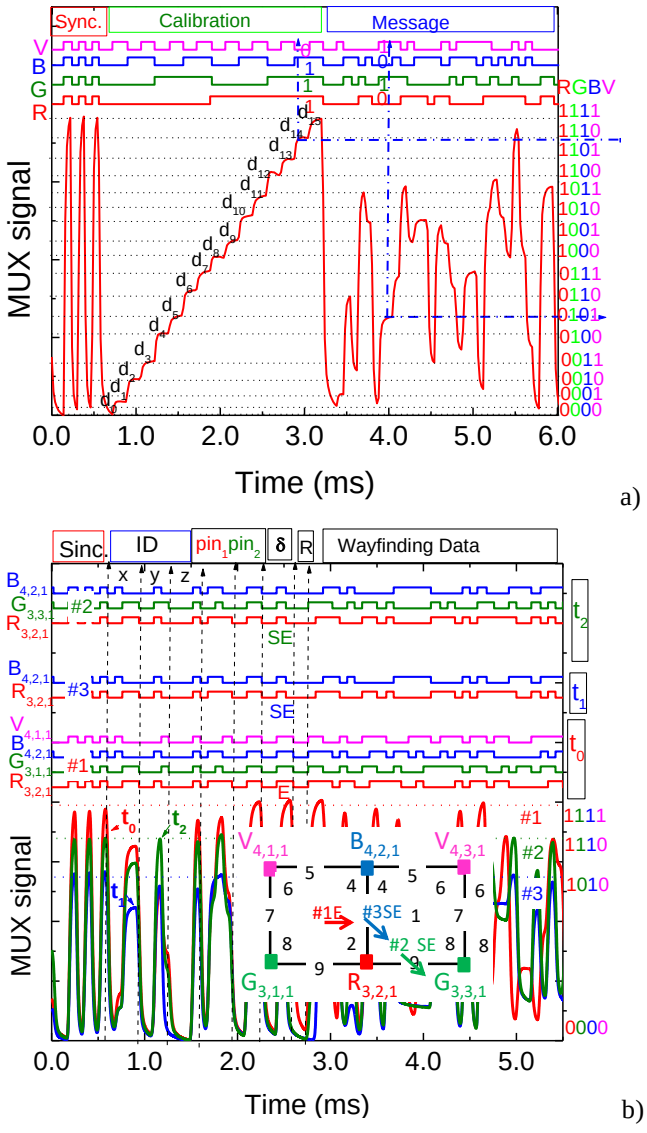

Figure 7. a) MUX/DEMUX signals of the calibrated cell. In the same frame of time a random signal (Message) is superimposed. b) Fine-grained indoor localization and navigation in successive instants. On the top the transmitted channels packets are decoded [R, G, B, V].

Due to the proximity of successive levels occasional errors occur in the decoded information. A parity check is performed after the word has been read [22]. The parity bits are the SUM bits of the three-bit additions of violet pulsed signal with two additional RGB bits and defined as:

$$P_R = V \oplus R \oplus B;\ P_G = V \oplus R \oplus G;\ P_B = V \oplus G \oplus B \quad (6)$$

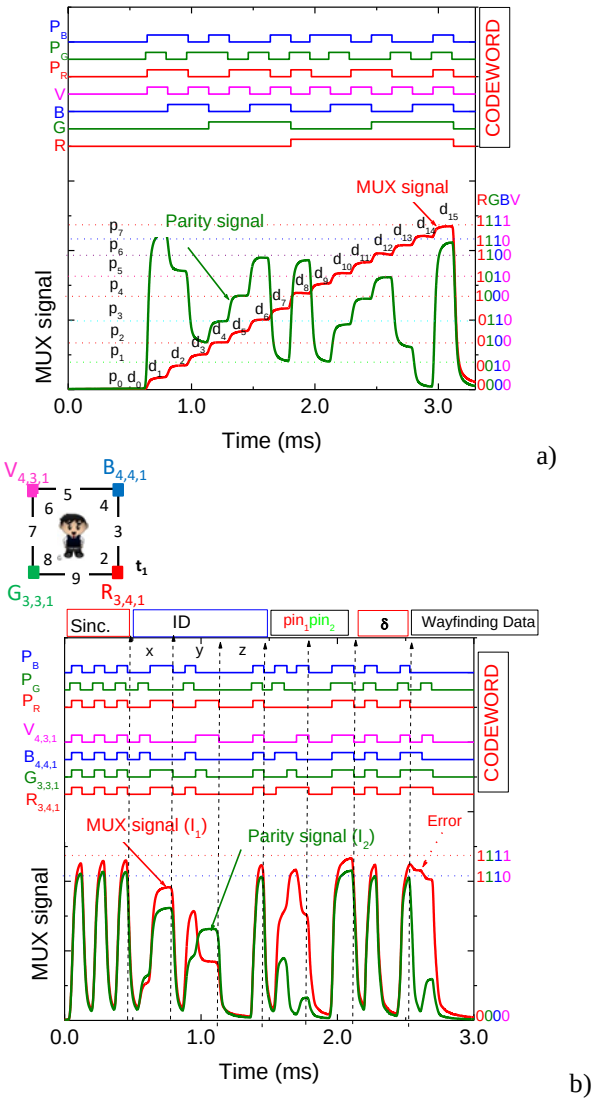

Figure 8. Code and parity MUX/DEMUX signals. On the top the transmitted channels [R G B V : P_R P_G P_B] are shown. a) Calibrated cell. b) Error control assigned to a request from user "7261" at $C_{4,3,1}$; #1 N.

In Figure 8a, the MUX signal that arises from the transmission of the four calibrated RGBV wavelength channels and the MUX signal that results from the generation of the synchronized parity MUX are displayed. On the top the seven bit word [R,G,B,V, P_R, P_G, P_B] of the transmitted inputs guides the eyes. The colors red, green, blue and violet were assigned respectively to P_R, P_G and P_B. For simplicity the received data ($d_{0\text{-}15}$ levels) is marked in the correspondent MUX slots as well as the parity levels marked as horizontal lines. On the top the decoded 7-bit coded word is exhibited. In the right side 4-bit binary codes assigned to the eight parity sublevels are inserted.

The traffic message is revealed by decoding MUX signals and considering the framestructure, pose, and transmitter type [19]. In Figure 8b, we illustrate how error control is achieved using check parity bits. A request from user "7261" is shown at $C_{4,3,1}$; #1 N, along with the matching parity signal. Results show that without check parity bits, decoding was difficult primarily when levels were close together (dotted arrow).

The study of optical interference was also briefly attempted and how it can affect a VLC communication link. Three types of optical sources were chosen due to their availability and their likelihood of existing near a real-world indoor VLC system: halogen light, fluorescent light, and LED light. Measuring the intensity of each optical source at R (624 nm), G (540 nm), B (480 nm) and V (405 nm) wavelengths, without optical interference as a reference point, the RGBV (Red-Green-Blue-Violet) components of each optical source raises or lowers the light gain at those wavelengths. As the calibration curve is used to define the 16 possible levels (d_0-d_{15}, Figure 7), optical interferences are negligible. A wide range of factors influence optical interference (such as angle of incidence, optical aperture, luminous intensity, etc.) and, while some success has been observed in nullifying the disruptive effects of optical interference on decoding with the signal-to-bit algorithm, the results were based on specific optical sources measured under certain non-rigorous conditions. Before any concrete conclusions can be drawn about the full impact of optical interference on a VLC system and how it can be minimized or counteracted, further studies will be necessary to complement these results.

B. Multi-person cooperative localization and guidance services

Bi-directional communication between VLC emitters and receivers is available at a VLC ready handheld device, through the control manager interconnected with a signboard receiver located at each unit cells (#1). These communications channels constitute the uplink (D2I) and downlink channels (I2D). Each user (D2I) sends to the local controller a "request" message with the pose, $q_i(t)$, (x,y,z, δ), user code (pin_1) and also adds its needs (code meeting and wayfinding data). For route coordination the CM, using the information of the network's VLC location capability, sends a personalized "response" message to each client at the requested pose with his wayfinding needs.

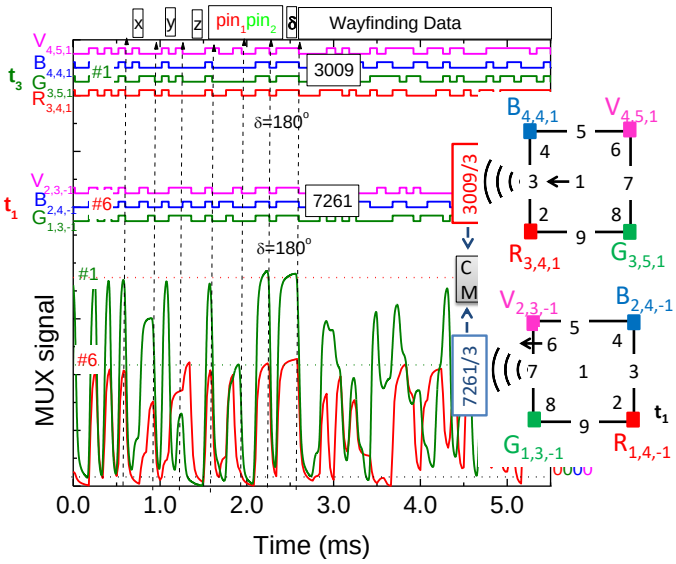

Figure 9. MUX/DEMUX signals assigned requests from two users ("3009" and "7261") at different poses ($C_{4,4,1}$; #1W and $C_{2,3,-1}$; #6 W) and in successive instants (t_1 and t_3).

In Figure 9, the MUX synchronized signals received by two users that have requested wayfinding services, at different times, are displayed. We have assumed that a user located at $C_{2,3,-1}$, arrived first (t_1), auto-identified as ("7261") and informed the controller of his intention to find a friend for a previously scheduled meeting (code 3). A buddy list is then generated and will include all the users who have the same meeting code. User "3009" arrives later (t_3), sends the alert notification ($C_{4,4,1}$; t_3) to be triggered when his friend is in his floor vicinity, level 1, identifies himself ("3009") and uses the same code (code 3), to track the best way to his meeting.

After this request (t_3), the buddy finder service uses the location information from both user' devices to determine the proximity of their owners (q_{ij} (t)) and sends a response message with the best route to the meeting.

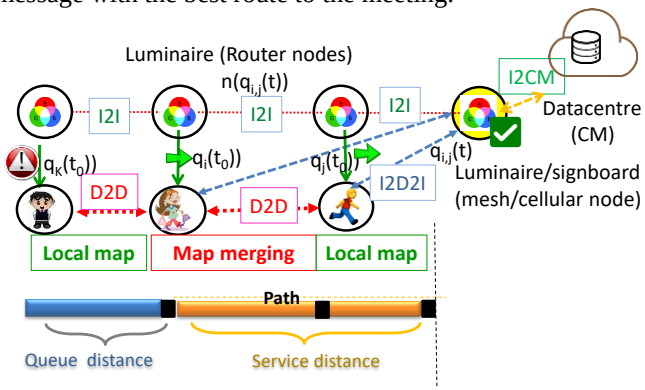

Figure 10. Graphical representation of the simultaneous localization and mapping problem using connectivity as a function of node density, mobility and transmission range.

The pedestrian movement along the path can be thought as a queue, where the pedestrians arrive at a path, wait if the path is congested and then move once the congestion reduces.

In Figure 10, a graphical representation of the simultaneous localization and mapping problem using connectivity as a function of node density, mobility and transmission range is illustrated. The following parameters are therefore needed to model the queuing system: The initial arrival time (t_0) and the path, respectively, defined as the time when the pedestrian leaves the previous path and the actual movement along the path, q_i (t, t'). Here, the service time is calculated using walking speed and distance of the path.

The number of service units or resources is determined from the capacity of the path, $n(q_i(x,y,z, \delta, t))$ and walking speed that depends on the number of request services, and on the direction of movement along the path $q_i(x,y,z, \delta, t)$. Since the number of service units is same as the capacity of the path, the queue size is theoretically zero.

Once appended by the CM (request message), the pedestrians are served immediately (response message). If the number of pedestrians exceeds the path capacity, a backlog is automatically formed until the starting node. The hybrid controller integrates the number of requests and individual positions received during the same time interval. Once the individual positions are known, q_i (t), the relative positions are calculated, q_{ij} (t). If the relative position is less than a threshold distance, a crowded region locally exists, and an alert message is sent for the users. This alert allows the CM to recalculate, in real time, the best route for the users, q_i (t,t'), that request wayfinding services avoiding crowded regions.

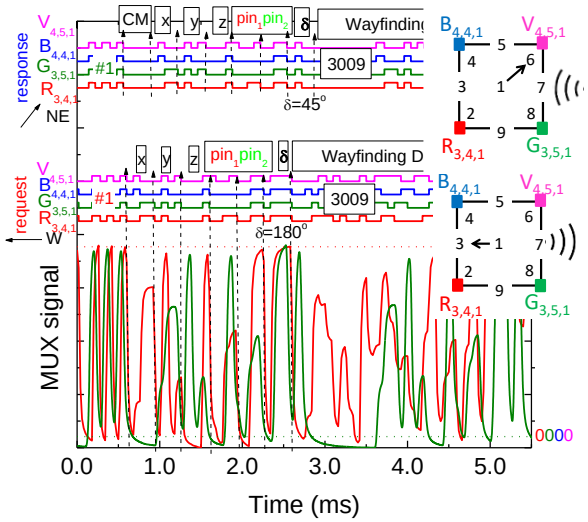

Figure 11. Request from user "3009" and response from the CM to him. On the top the transmitted channels packets are decoded [Xi,j,k].

An example of the MUX signals assigned to a request/response received by user "3009" during his path to reach user "7261" is displayed in Figure 11. In the top of the

figure, the decoded information is shown and the simulated scenario is inserted to guide the eyes.

The "request" message includes, beyond synchronism, the identification of the user ("3009"), its address and orientation ($C_{4,4,1}$, #1W) and the help requested (Wayfinding Data). Since a meet-up between users is expected, its code was inserted before the right track request. In the "response", the block CM identifies the sender [0000] and the next blocks the cell address ($C_{4,4,1}$), the user (3009) for which the message is intended and finally the requested information: meeting code 3, orientation NE (code 4) and wayfinding instructions. Every time a user switches floors he has to notify the CM and a new alert is received to optimize the way. In response to the estimated relative pose position, $q_{i,j}$ (t), between the users with the same meeting code, the CM sends a new alert that takes into account the occupancy of the service areas along the paths, q_i (x,y,z, δ, t), which optimizes the path without crowding the users.

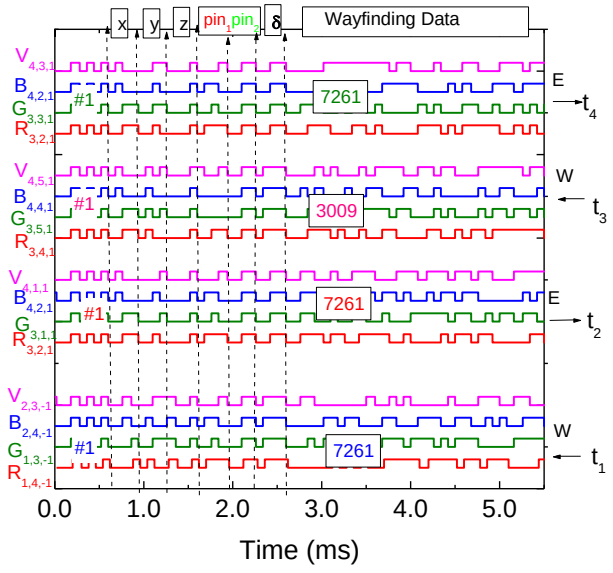

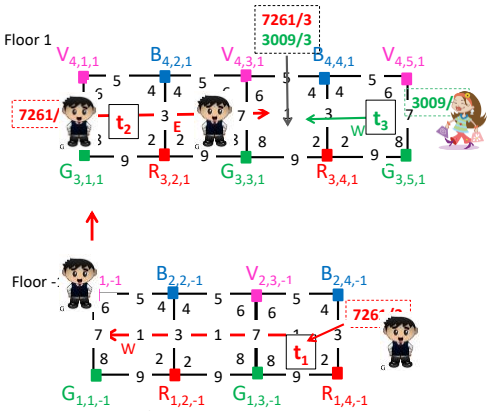

Figure 12. Decoded messages from the two users as they travel to a pre-scheduled meeting.

In Figure 12, the decoded messages from the two users as they travel to the pre-scheduled meeting is displayed. At the botton the geolocation of both user is illustrated.

Decoded data shows that user "7621" starts (t_1) his journey on floor -1, $C_{2,3,-1}$; #1W, goes up to floor 1 in $C_{2,1,-1}$ and at t_2 he arrives at $C_{4,1,1}$ heading for E. During his journey, user "3009" from $C_{4,4,1}$ #1 asks the CM (t_3) to forward him to the scheduled meeting and follows course to W. At t_4 both friends join in $C_{4,3,1}$.

IV. Conclusions

A cooperative indoor VLC localization and navigation system is proposed. In a multi-level building scenario, the architecture of the system and the protocol of communication were defined. Bi-directional communication between the infrastructure and the mobile receiver was analyzed.

According to global results, the location of a mobile receiver is found in conjunction with data transmission. VLC's dynamic LED-aided navigation system is designed to give users accurate route guidance and enable navigation and geotracking. The multi-person cooperative localization system detects crowded regions and alerts the user to reschedule meetups, as well as provides guidance information. With those alerts, the CM can recalculate, in real time, the best route for users requesting wayfinding services, avoiding crowded areas.

Acknowledgements

This work was sponsored by FCT – Fundação para a Ciência e a Tecnologia, within the Research Unit CTS – Center of Technology and Systems, reference UIDB/00066/2020. The IPL/2022/POSEIDON_ISEL Project was also acknowledged.

References

[1] M. Vieira, M. A. Vieira, P. Louro, A. Fantoni, and P. Vieira, "Indoor Guidance Services through Visible Light Communication," ALLSENSORS 2022: The Seventh International Conference on Advances in Sensors, Actuators, Metering and Sensing Copyright (c) IARIA, 2022. ISBN: 978-1-61208-987-4, pp. 8-12.

[2] E. Ozgur E. Dinc, and O. B. Akan, "Communicate to illuminate: State-of-the-art and research challenges for visible light communications," Physical Communication, vol. 17, pp. 72–85, 2015.

[3] C. Yang and H. R. Shao, "WiFi-based indoor positioning," IEEE Commun. Mag., vol. 53, no. 3, pp. 150–157, Mar. 2015.

[4] D. Tsonev, et al. "A 3-Gb/s single-LED OFDM-based wireless VLC link using a Gallium Nitride μLED," IEEE Photon. Technol. Lett., vol. , no. 7, pp. 637–640, 2014.

[5] D. O'Brien, et al., "Indoor visible light communications: challenges and prospects," Proc. SPIE 7091, 709106, pp. 60-68, 2008.

[6] H. -H. Liu and Y.-N Yang, "WiFi-based indoor positioning for multi-floor environment," Proceedings of the IEEE Region 10 Conference on Trends and Development in

Converging Technology Towards (TENCON '11)November 2011Bali,Indonesia59760110.1109/TENCON.2011.6129175 2-s2.0-84863014825, pp.597-601, 2011.

[7] Y. Wang, H. Li, X. Luo, Q. Sun, and J. Liu "A 3D Fingerprinting Positioning Method Based on Cellular Networks," International Journal of Distributed Sensor Networks, p. 248981, 2014.

[8] M. Vieira, M. A. Vieira., P. Louro, P. Vieira, and A. Fantoni, "Fine-grained indoor localization: optical sensing and detection," Proc. SPIE 10680, Optical Sensing and Detection V, 106800H, 9 May 2018.

[9] A. Jovicic, J. Li, and T. Richardson, "Visible light communication: opportunities, challenges and the path to market," Communications Magazine, IEEE, vol. 51, no. 12, pp. 26–32, 2013.

[10] M. A. Vieira, M. Vieira, P. Louro, V. Silva, and P. Vieira, "Optical signal processing for indoor positioning using a-SiCH technology," Opt. Eng. Vol. 55, no. 10, 107105, 2016.

[11] M. A. Vieira, P. Louro, M. Vieira, A. Fantoni, and A. Steiger-Garção, "Light-activated amplification in Si-C tandem devices: A capacitive active filter model," IEEE Sensor Journal, 12, no. 6, pp. 1755-1762, 2012.

[12] S. B. Park, et al., "Information broadcasting system based on visible light signboard," presented at Wireless and Optical Communication 2007, Montreal, Canada, 2007.

[13] M. Vieira, M. A. Vieira, P. Louro, P. Vieira, and A. Fantoni, "Light-emitting diodes aided indoor localization using visible light communication technology," Opt. Eng., vol. 57, no. 8, 087105, 2018.

[14] M. A. Vieira, M. Vieira, P. Louro, and P. Vieira, "Bi-directional communication between infrastructures and vehicles through visible light," Proc. SPIE 11207, Fourth International Conference on Applications of Optics and Photonics, 112070C (3 October 2019); doi: 10.1117/12.2526500, 2019.

[15] Y. Zhu, W. Liang, J. Zhang, and Y. Zhang, "Space-Collaborative Constellation Designs for MIMO Indoor Visible Light Communications," IEEE Photonics Technology Letters, vol. 27, no. 15, pp. 1667–1670, 2015.

[16] H.T. Friis, "A note on a simple transmission formula" Proc. IRE34, pp. 254–256, 1946.

[17] R. Rajesh, "Dynamic Vehicle and control" Mechanical Engineering Series, ISBN 978-1-4614-1433-9 . 2012.

[18] J. Ackermann, J. Guldner, W. Sienel, R. Steinhauser, and V. Utkin, "Linear and Nonlinear Controller Design for Robust Automatic Steering, " IEEE Transactions on Control Systems Technology , vol. 3, no. 1, pp. 132 – 143, Mar. 1995), ,DOI: 10.1109/87.370719, 1995.

[19] M. Vieira, M.. A. Vieira, P. Louro, A. Fantoni, and P. Vieira, "Geolocation and communication in unfamiliar indoor environments through visible light", Proc. SPIE 11706, Light-Emitting Devices, Materials, and Applications XXV, 117060P (March 2021); https://doi.org/10.1117/12.2576904.

[20] M. Vieira, M. A. Vieira, P. Louro, A. Fantoni, P. Vieira, "Dynamic VLC navigation system in Crowded Buildings," International Journal On Advances in Software, vol. 14, no. 3&4, pp. 141-150, 2021.

[21] M. Vieira, M.A. Vieira, P. Louro, P.Vieira, "A Visible Light Communication System to Support Indoor Guidance. In: Camarinha-Matos, L.M., Ribeiro, L., Strous, L. (eds) Internet of Things. IoT through a Multi-disciplinary Perspective. IFIPIoT 2022. IFIP Advances in Information and Communication Technology, vol 665, pp. 235-252. Springer, Cham. https://doi.org/10.1007/978-3-031-18872-5_14, 2022.

[22] M. A. Vieira, M, Vieira, V. Silva, P. Louro, and J. Costa, "Optical signal processing for data error detection and correction using a-SiCH technology," Phys. Status Solidi C, vol. 12, no. 12, pp. 1393–1400, 2015.

Use of Footprint Maps to Support Positioning and Guidance in Visible Light Communication Technology

Paula Louro, Manuela Vieira, Manuel Augusto Vieira
DEETC/ISEL/IPL,
R. Conselheiro Emídio Navarro, 1959-007
Lisboa, Portugal

CTS-UNINOVA
Quinta da Torre, Monte da Caparica, 2829-516,
Caparica, Portugal
e-mail: plouro@deetc.isel.pt, mv@isel.ipl.pt,
mvieira@deetc.isel.pt

***Abstract*— Due to the general, worldwide need for communication, Visible Light Communication (VLC) has become a research topic today. In comparison to other wireless technologies (such as Wi-Fi), this technology combines lighting and communication, enabling high data rates and reliability. In this paper VLC is used to establish different optical communication links for bidirectional communication between infrastructures and vehicles, namely Infrastructure-To-Vehicle (I2V) and Vehicle-To-Infrastructure (V2I). VLC is used to provide guidance and management services for autonomous robot navigation inside an automated warehouse. Specific coding schemes are used in each optical link. The I2V link uses RGB white LEDs to simultaneously modulate the emitters embedded in each LED, allowing wavelength division multiplexing of optical signals transmitted via this link. The detection is based on an a-SiC:H pin-pin photodetector with tunable sensitivity in the visible range. The impact of parity check bits on bit error rate is discussed for different indoor communication scenarios.**

Keywords- Visible Light Communication; Indoor guidance; White LEDs; Lambertian model; navigation cell.

I. INTRODUCTION

This paper is an extension of work originally presented in ALLSENSORS 2022 [1] that provided preliminary results of the use of footprint maps to support positioning and guidance under visible light communication technology. This work discusses the use of the footprint maps for this purpose and the importance of proper decoding methods.

Indoor positioning can be addressed by several techniques, such as Wi-Fi, Assisted GPS (A-GPS), Infrared, Radio Frequency Identification (RFID), and many other technologies [2][3]. Visible Light communication (VLC) is also an alternative, enhanced accuracy technology. VLC operates with visible light extending from 400 nm up to 750 nm [4][5]. VLC systems use modulated LEDs to transmit information [6]. Due to its characteristics, LEDs [7] can be switched very fast to produce modulated light in high frequencies, allowing data transmission in high speed. For lighting purposes, energy saving demands the use of white LEDs [8][9], either based on blue emitter coated with a phosphor layer or based on polychromatic emitters. Phosphor-based LEDs usually consist of a blue LED chip covered in a yellow phosphor layer. Due to the long relaxation time of the phosphor, when this LED is used for VLC, the modulation bandwidth is limited, thereby limiting the transmission capacity. Using a blue filter before the receiver unit can increase the LED modulation bandwidth by eliminating the slow response of the yellow light component [10][11]. Although tri-chromatic LEDs are more expensive, they provide more bandwidth due to the independent modulation of each chip of a monolithic device.

The receiver unit of VLC systems usually includes silicon-based photodiodes, as these devices operate in the visible region of the spectrum, or CMOS image sensors [12][13].

In this paper we propose the use of a multilayered a-SiC**:**H [14] [15] device to perform the photodetection of the optical signals generated by white trichromatic RGB LEDs [16], [17]. The system was designed for positioning and guidance [18][19], and the transmitters of each white LED were specifically modulated at precise frequencies and coding bit sequences [20][21].

The optical VLC channel is characterized through the prediction of the channel gain, taking into consideration emitter characteristics, optical channel features and receiver properties. The Lambertian model is used for LED light distribution and MatLab simulations are used to infer the signal coverage of the LED in the illuminated indoor space [22][23]. The decoding strategy of the multiplexed signals demands system calibration for accurate regulation of each photocurrent level [24][25] and preferably the use of bit error control strategies, which are also discussed. For each link, different codification schemes are proposed using On-Off keying modulation.

The proposed lighting and positioning/guidance system involves wireless communication, computer-based algorithms, smart sensor, and optical sources network, which constitutes a transdisciplinary approach framed in cyber-physical systems.

The paper is organized as follows. After the introduction (Section I), the general description of the system is presented in Section II. In Section III, the communication protocol and the encoding/decoding techniques are analyzed and discussed. At last, conclusions are addressed in Section IV.

II. VLC SYSTEM GENERAL DESCRIPTION

The VLC system is composed by the transmitter and the receiver modules, located at the infra-structure and at the mobile vehicle. Two optical links are established between the lamps and the vehicles, for I2V and V2I transmission. The optical source of the transmitter at infrastructure consists of four white RGB LEDs, while at a vehicle it is a multicolor LED or a single-color LED placed at the top. The sensor device used for the detection of the optical signals is a monolithic heterojunction composed of two pin structures [26]. As a result of its narrow thickness (200 nm) and higher bandgap (2.1 eV), the front pin a-SiC:H photodiode is responsible for the device's sensitivity to short wavelengths of the visible range (400 - 550 nm). The back pin a-Si:H structure operates in the complementary past of the visible range, collecting the long wavelengths (520 nm - 700 nm) [27]. The illumination window is established on the front photodiode. The use of steady state light as background light provides an enhancement of the electrical field of the front pin photodiode and the amplification of the generated photocurrent signal due to long wavelength light.

A. Transmitter configuration

For every channel of the I2V and V2I links, synchronous transmission based on a 64 bits data frame was used. In Figure 1 a) it is displayed the configuration of the LED lamp with four RGB white LEDs used in the I2V link. A uniform white light is provided in the indoor area by all three emitters (red, green, and blue). However, only specific emitters are modulated at a frequency imperceptible to the human eye. Each of these lamps illuminates an area with full radial coverage as shown Figure 1 b).

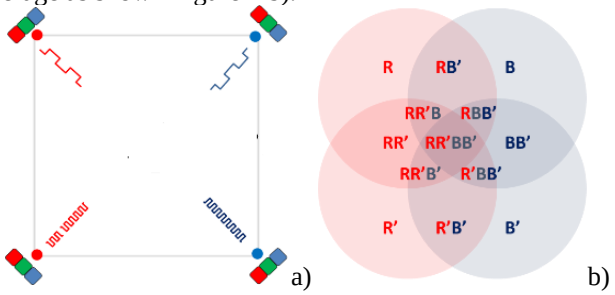

Figure 1. Configuration of the VLC emitter: a) 4 RGB white LEDs; b) coverage area of each modulated emitter.

The illuminated area corresponds to the coverage area of each lamp, defining a unit cell for the vehicle navigation along the space. The modulated emitters are the red junctions of the LEDs placed at the left side and the blue junctions of the LEDs at the right side.

For the proposed system, the commercial white LEDs were designed for illumination purposes, exhibiting a wide half intensity angle ($\phi_{1/2}$) of 120º. Thus, the Lambertian order *m* is 1. The coverage range and radiation pattern of the LED light is affected by the half intensity angle, such that narrower $\phi_{1/2}$ increases the illumination range. In Figure 2 it is displayed the luminous intensity of the red, green, and blue optical emitters of the white RGB commercial LEDs used in this system.

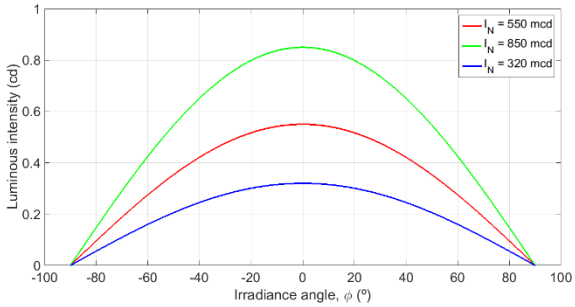

Figure 2. Distribution of luminous intensity for the red, green, and blue emitters.

For the maximum luminous intensity in the axial direction (I_N) it was considered the average values stated in the datasheet specifications [28]. As it is shown in Figure 2, the luminous intensity varies with the direction, presenting a maximum at the axial direction (0º) and half of the maximum at $\phi_{1/2}$= ± 60º.

In Figure 3 it is plotted the normalized output spectra of the RGB white LEDs driven with a biasing current of 3 mA.

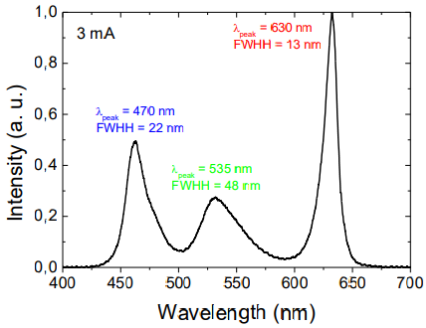

Figure 3. Output normalized spectrum of the RGB white LED.

The output spectra cover the wavelengths assigned to the blue, green and red regions, with wavelengths centered, respectively at 470 nm, 535 nm and 630 nm. The full width half height of each peak (FWHH) is 22 nm for the blue chip, nearly 48 nm for the green and 13 nm for the red chip. Usually, the FWHH of LED devices increases with the wavelength. However, as this is a white LED, the magnitude and width of each RGB peaks are optimized for the white. The green component is the lowest because the human eye has a maximum sensitivity at 530 nm.

Table I summarizes the main optical characteristics of the optical sources of the VLC transmitter.

TABLE I. OPTICAL CHARACTERISTICS OF THE WHITE LEDS AT 25 ºC.

Central wavelength (nm)	620	530	470
Luninous intensity (mcd)	628	980	340
Linewidth @ 20 mA	24	38	28
Half intensity angle (°)	± 60	± 60	± 60

B. Channel characterization

LEDs are modeled as Lambertian sources with uniform distribution of luminance in all directions, and luminous intensity dependent on the direction. The luminous intensity for a Lambertian source is given by the following equation [29]:

$$I(\phi) = I_N \cos^m(\phi) \quad (1)$$

where m is the order derived from a Lambertian pattern, I_N is the maximum luminous intensity in the axial direction and ϕ is the angle of irradiance. The Lambertian order m is given by:

$$m = -\frac{\ln(2)}{\ln(\cos(\phi_{1/2}))} \quad (2)$$

The Lambertian order m indicates the LED's half-power angle. The semi-angle represents the area illuminated by the LED radiation pattern. Generally, a small m (around 1) indicates a wide illumination region, whereas a high m relates to a highly focused illumination region. Thus, m is a measure of light source spatial directivity. In this case, as the half intensity angle ($\phi_{1/2}$) is of 60º, the Lambertian order m is 1.

The light signal is received by the photodetector, generates a binary sequence of the received signals and converts data into the original format. It is assumed Line of Sight (LoS) conditions, which consider that the signal propagation occurs in a direct path from the source to the receiver.

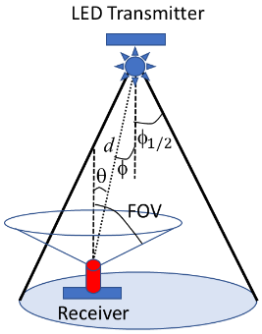

Figure 4. Transmitter and receiver relative position.

Figure 4 shows the relative position of the transmitter and receiver units with specification of the geometrical parameters needed to infer the signal coverage of the LED in the illuminated indoor space [30].

The channel gain (G) of the VLC link is given by equation [31]:

$$G = \frac{(m+1)A}{2\pi d^2} I_N \cos^m(\emptyset)\cos(\theta) \quad (3)$$

where A is the area of the photodetector, d is the distance between the emitter and the receiver, and FOV is the field of view of the detector (angular extension for signal detection).

In Figure 5 it is displayed the predicted received power of the emitters of the white RGB LED transmitter.

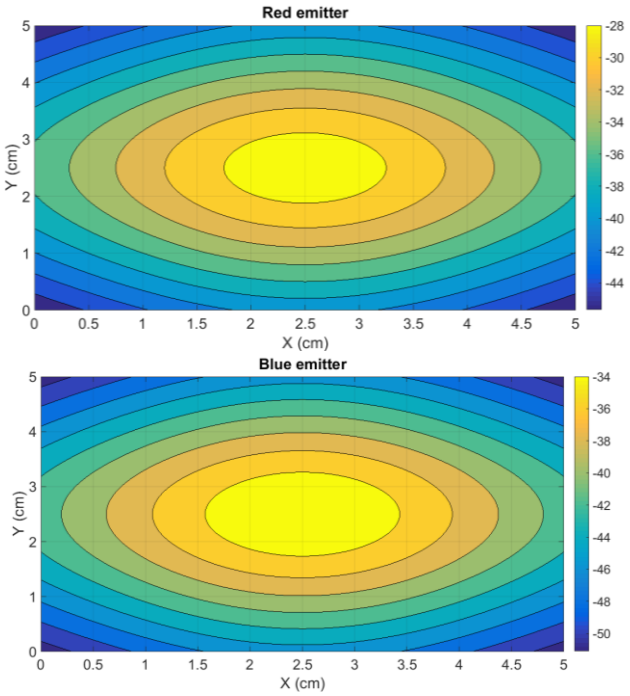

Figure 5. Received power (dBm) the red and blue emitters of the white RGB LED transmitter.

C. Footprint maps

Figure 6 illustrates the coverage map produced when only the red and blue emitters of each LED are used for data transmission. This region allows the definition of the unit navigation cell related to each luminaire of the illuminated space.

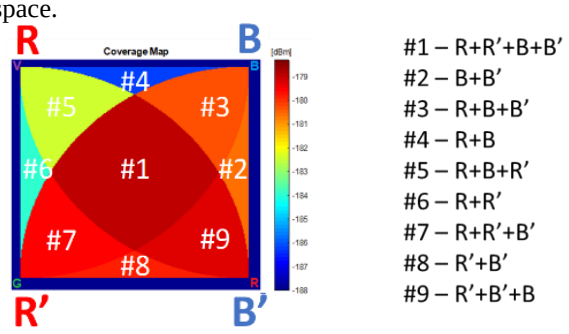

Figure 6. Coverage map of the fine-grain footprint inside the navigation cell, considering as VLC optical sources the top red and bottom blue emitters.

In each unit navigation cell, any receiver will be able to identify the emission lamp and make a correspondence to the spatial position inside the warehouse. By modulating the red and blue emitters of each lamp, the optical pattern created within each navigation cell can enhance position accuracy. Inside the navigation cell, top emitters (labelled R and B) point north, bottom emitters (R' and B') point south and left (R and R') and right (B and B') emitters point west and east, respectively.

Based on this assumption, the RB' optical pattern corresponds to the north direction, R'B' to the south, RR' to the west and BB' to the east. The intercardinal directions inside the navigation cell correspond to RR'B (northwest), RBB' (northeast), RR'B' (southwest) and R'BB' (southeast). In this coverage map the optical signal produced by each modulated LED confers a maximum of delivered power signal at the central region of the cell, that receives contribution from four modulated channels. The regions at the corners contain optical signals from three LEDs, exhibiting a decrease on the received power signal, while the side regions correspond to the lowest values of received power. Each of these regions constitute footprints of the delivered power. Each footprint region labelled as #1, #2, …, #9 is assigned to the correspondent optical excitation illustrated on the right side of Figure 6. Using adjacent LED lamps to light the indoor space, different navigation cells are enabled by each lamp. The identification of each lamp is provided by a specific code.

D. Coding

In Figure 7 it is displayed the data frame structure the bi-directional communication I2V and V2I.

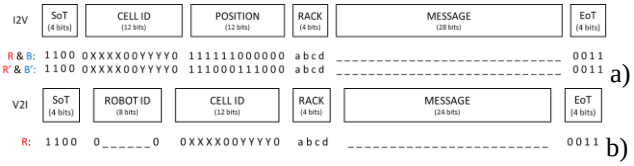

Figure 7. Data frame structure the communication: a) I2V and b) V2I channels.

Data frames are words of 64 bits composed each of six blocks. First and last blocks, labelled respectively as SoT (Start of Text) and EoT (End of Text) are used to trigger synchronization of the transmitter and receptor in each link. In the I2V link, there are also the blocks CELL ID, POSITION, RACK and MESSAGE. Identification of the unit cell is given by the block CELL ID. The format of the word code is 0XXXX00YYYY0, where XXXX addresses the line and YYYY the column of the unit navigation cell. Block POSITION provides information about which emitters are being detected by the mobile vehicle and thereby enables the vehicle to know its relative position within the navigation cell. The block RACK contains information about the stock stored inside the rack, addressing different sections. The MESSAGE block (32 bits) enables the possibility of transmitting a random message to the vehicle.

In the V2I link a single LED is used to transmit information from the vehicle to the infrastructure, namely information about items being removed from the rack within the navigation cell to the shipping station. The code word contains the blocks ROBOT ID, CELL ID, RACK and MESSAGE, besides SoT and EoT blocks. The blocks ROBOT ID and CELL ID encode the identification of the transmitting vehicle and of the receiver infrastructure. The RACK block identifies the specific rack from where items are being removed and the MESSAGE block encodes the item and quantity being removed.

E. Receiver configuration

The VLC receiver device of the system is a photodiode able to measure both pulsed and steady light sources, by converting the optical power to an electrical current, which depends on incident light power and wavelength. The photodiode is a dual sandwich pin photodetector with an a-Si:H pin structure mounted above an a-SiC:H pin structure, allowing the device to be used over the full a-Si:H and a-SiC:H wavelength ranges (Figure 8).

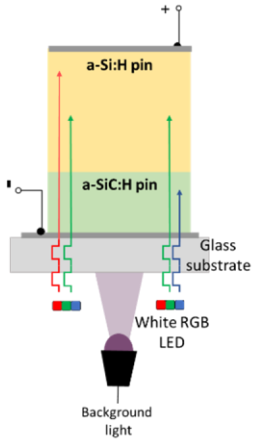

Figure 8. VLC sensor device: based on two stacked pin photodiodes based on a-SiC:H and a-Si:H.

It operates in the full range of the visible spectrum, with a spectral sensitivity that can be controlled externally using steady state light [32]. The device is housed on a glass substrate with one anode and one cathode connections. It is operated under reverse bias to improve collection efficiency. It is a large area device with a sensitive area of 1 cm^2 which contributes to the collection efficiency of light, and at the same time induces capacitive effects prone to limit speed operation.

The intrinsic layer materials used in each pin photodiode of the device and the thickness of each absorption layer provide different absorption mechanisms due to the specific material bandgaps. The used configuration delivers high absorption of short wavelength light in the front photodiode (a-SiC:H) and high absorption of the long wavelengths in the back photodiode (a-Si:H). Intermediate wavelengths are absorbed by both photodiodes. The use of steady state light as background light enhances the electrical field of the front a-SiC:H photodiode and amplifies the generated photocurrent signal produced under long wavelength light incidence.

III. RESULTS AND DISCUSSION

In the V2I link a single emitter is used to transmit information from the mobile robot to the LED infrastructure. In Figure 9 it is displayed the output signal due to the optical signal transmitted by the mobile robot after removing items

from a specific rack. On the top it is displayed the optical signal with the transmitted bit sequence. As this V2I link uses a single emitter, the photocurrent signal, when under line-of-sight condition, follows the pattern of the single transmitted optical signal. Thus, decoding is a simple process, limited only by the photodiode sensitivity at low illumination conditions.

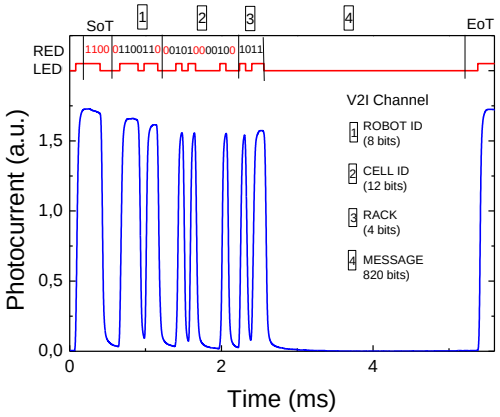

Figure 9. Output signal transmitted by the robot to the infrastructure after removal of items from the rack. On the top it displayed the transmitted optical signal.

As shown in the figure, bits in red color, either set to 1 or to 0, cannot be changed in this channel. Bits in black color are those that define the specific communication conditions. In this case, the blocks of the coded 64-bits word can be easily decoded. Bits of the ROBOT ID are 01100110, corresponding to the identification code 118 (decimal representation). The CELL ID provides for the decoded bits, the number 001010000100, which corresponds to line 5 and column 2. Bits of the RACK block are 1011, representing that items from the first and third racks were removed when the vehicle moved in the forward lane.

In the I2V link, the use of four emitters to transmit the coded information generates 16 photocurrents levels, assigned to 16 different optical excitations. These levels are dependent on the optical intensity at the reception end, however, its relative position is assumed to be constant. This supports the use of a calibration curve to demultiplex the signal, decodes the transmitted bits and enables identification of the input optical signals. In Figure 10 it is displayed the calibration curve, showing the 16 output levels assigned to each input optical state. The driving current of each LED emitter was adjusted to provide different levels of photo excitation.

On the right side of the picture, it is shown the label of the modulated emitters that correspond to each photocurrent level. The decoding methodology based on the calibration curve may result in some error mismatch when the photocurrent levels are too close. It is important to mention that only 9 of these 16 levels are used to infer the position using the footprint maps. Thus, the correct decoding of these levels is crucial to support positioning.

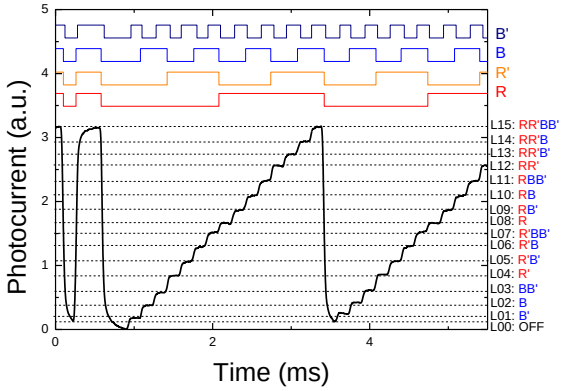

Figure 10. Calibration photocurrent signal using two red and two blue optical signals (on the top it is displayed the waveform of the emitters modulation state).

To increase the accuracy of the decoding task, bit error detection with parity check bits can be used. Parity bits (P1, P2, P3) assigned to the 4 transmission channels (R, R', B, B') are evaluated using a simple algorithm that sums up the bits transmitted by 3 of the channels:

$$P1 = R + R' + B'$$
$$P2 = R' + B + B' \quad (4)$$
$$P3 = R + B + B'$$

In Figure 11 it is displayed the parity check bits evaluated by equation (1) for the transmission of the bit sequences plotted in Figure 10. The parity check bits sequences (P1, P2 and P3) are transmitted, respectively, by the R, R' and B emitters.

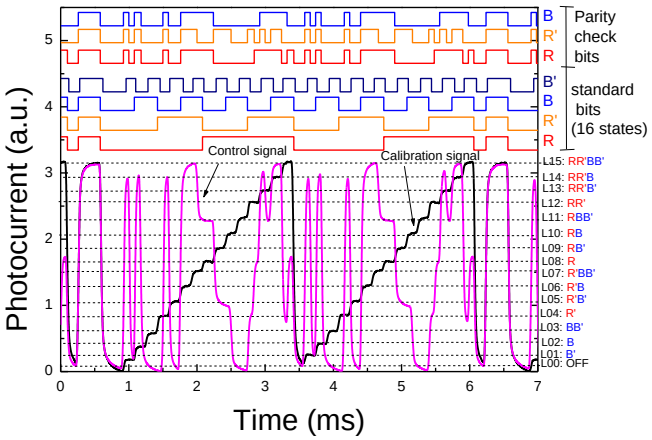

Figure 11. Calibration data and correspondent error control signal obtained by the transmission of the parity check bits.

Results show that the error control signal can be used to help on the decode process when photocurrent levels are very close. Under these circumstances, the use of parity check bits can detect and correct errors without the need to discard the transmitted data from the specific error bit and re-transmit it again.

In Figure 12 it is displayed the photocurrent signal acquired along the forward lane at positions under the coverage of RR'BB'. In superposition it is displayed the calibration grid. At the top it is displayed the input optical signals (R, R', B and B').

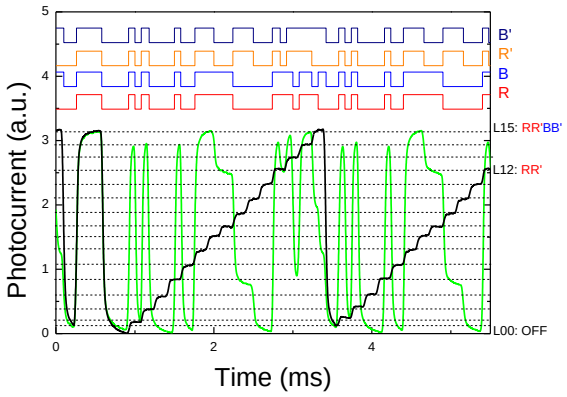

Figure 12. Photocurrent signal acquired along the forward path at cell central position under the coverage of RR'BB'.

The comparison of the output signal with the calibration curve allows the decode of the signal and identification of the receiver's position. Bit decoding of the multiplexed signal resulted for the CELL ID block the word 001010000100 (every 4 transmitters), corresponding to line 5 and column 2, for the POSITION block to the word 111111000000 from R and B transmitters and word 111000111000 from R' and B' transmitters, which indicates that the vehicle is at the center of the navigation cell. For the RACK block it is decoded the words 1110 from R and B transmitters and 1011 from R' and B' transmitters, which means that all racks of the cell are available with exception to the second rack in forward direction.

In Figure 13a) it is displayed the error control signal obtained with parity check bits of the transmitted signal of the I2V link shown in Figure 12.

The use of the calibration curve for decoding the multiplexed signal, demands a periodic transmission of the 16 possible combinations of the 4 optical signals to provide update of the calibration data and ensure correct output signal assignment. In this application, speed is not a critical issue, and this procedure does not overload the transmission efficiency. However, it can be discarded or done with less frequency when the accuracy of the decoding is increased using parity check bits.

The system is also feasible to be enhanced using feedback control for adjustment of the LED driving currents when the output photocurrent levels generated by the photodiode become too close. This procedure would minimize decoding errors due to parasitic effects such as optical intensity variations caused by to multiple reflections, light dispersion, or other light sources. Thus, the ambient light would not affect the proposed methodology.

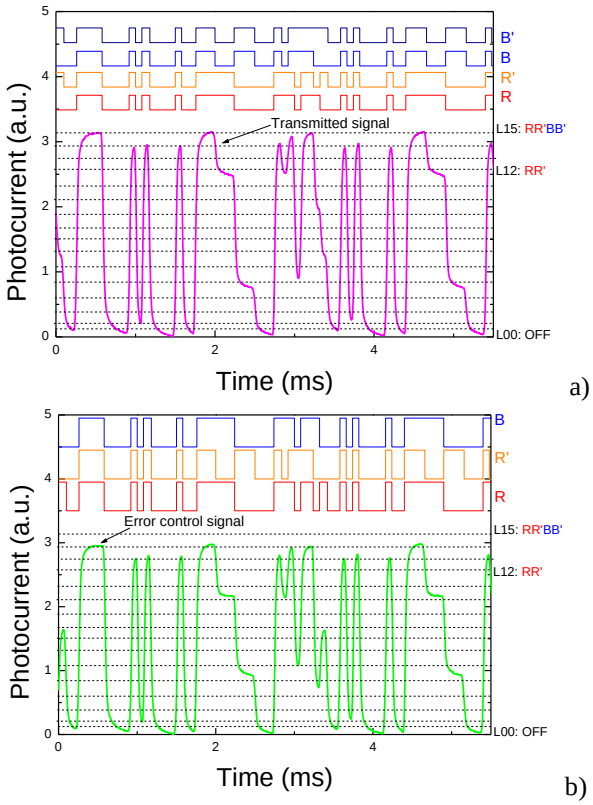

Figure 13. a) Transmitted signal by the I2V link and b) correspondent error control signal.

In addition to this bit error control strategy that improves the communication robustness, other coding schemes can be implemented, such as Manchester. OOK is a valuable modulation scheme in VLC due to its low complexity and ease of implementation. However, it may include flickering effects, which disturb the illumination distribution and even the communication under low dimming conditions.

The use of Manchester codes demands the use of two bits to transmit each symbol, which halves the data rate. However, it is prone to cause less hysteresis effects ensuring a stable calibration curve in better agreement with the level of each optical excitation.

IV. CONCLUSIONS

Bi-directional communication using VLC in both downlink and uplink channels has been addressed in a autonomous vehicle guidance system. The proposed indoor application deals with infrastructure to vehicle (I2V) and vehicle to infrastructure (V2I) communication in a warehouse. The vehicle moves autonomously through the warehouse transporting goods from the carts to the packaging station. The transmitted data is encoded in a 64 bits word, defined using specific data frames in communication channel. Codification of the optical signals ensured synchronization between frames. The code word of each channel was designed to ensure synchronization between

frames, to transmit information of the transmitter identification and of spatial location. Experimental evaluation demonstrated that the decoding solution can provide robust communications, especially if automatic bit error control is implemented in the optical domain. The optical sources using trichromatic LEDs were fully characterized by the Lambertian model adapted to the specifications of each LED. This provided the definition of footprint maps, necessary to enhance the accuracy of the position inside each navigation cell.

In addition, to the mentioned above relating the decoding process, other coding schemes may be implemented in future developments of the proposed system, namely Manchester codes.

ACKNOWLEDGEMENTS

This work was sponsored by FCT – Fundação para a Ciência e a Tecnologia, within the Research Unit CTS – Center of Technology and systems, reference UID/EEA/00066/2020 and IPL/2022/POSEIDON_ISEL.

REFERENCES

[1] P. Louro, M. Vieira, M. A. Vieira, "VLC Footprint Maps for Positioning and Guidance", ALLSENSORS 2022: The Seventh International Conference on Advances in Sensors, Actuators, Metering and Sensing, June 26-30, Porto, Portugal. ISBN: 978-1-61208-987-4, pp. 25-29.

[2] R. Mautz, "Overview of Current Indoor Positioning Systems", Geodesy Cartogr., vol. 35, pp. 18–22, 2009.

[3] Y. Gu, A. Lo, and I. Niemegeers, "A Survey of Indoor Positioning Systems for Wireless Personal Networks," IEEE Commun. Surv. Tutor., vol. 11, pp. 13–32, 2009.

[4] A. M. Căilean and M. Dimian, "Current Challenges for Visible Light Communications Usage in Vehicle Applications: A Survey", IEEE Communications Surveys & Tutorials, vol. 19, no. 4, pp. 2681-2703, 2017.

[5] M. Z. Chowdhury, M. T. Hossan, A. Islam, and Y. M Jang, "A Comparative Survey of Optical Wireless Technologies: Architectures and Applications", IEEE Access, vol. 6, pp. 9819-9840, 2018.

[6] G. Cossu, A. M. Khalid, P. Choudhury, R. Corsini, and E. Ciaramella, "3.4 Gbit/s Visible Optical Wireless Transmission Based on RGB LED," Optics Express, vol. 20, pp. B501–B506, 2012.

[7] M. Kavehrad, "Sustainable Energy-Efficient Wireless Applications Using Light", IEEE Communications Magazine, vol. 48, no. 12, pp. 66-73, 2010.

[8] E. F. Schubert and J. K. Kim, "Solid-state light sources getting smart", Science, vol. 308, no. 5726, pp. 1274-1278, 2005.

[9] J.-Y. Sung, C.-W. Chow, and C.-H Yeh, "Is blue optical filters necessary in high speed phosphor-based white light LED visible light communications?", Optics Express, vol. 22, no. 17, pp. 20646-20651, 2014.

[10] H. Le Minh et al., "High-speed visible light communications using multiple-resonant equalization," IEEE Photon. Technol. Lett., vol. 20, no. 14, pp. 1243–1245, 2008.

[11] A. M. Khalid, G. Cossu, R. Corsini, P. Choudhury, and E. Ciaramella, "1-Gb/s transmission over a phosphorescent white LED by using rate-adaptive discrete multitone modulation", IEEE Photon. J., vol. 4, no. 5, pp. 1465–1473, 2012.

[12] Z. Zhou, M. Kavehrad, and P. Deng, "Energy efficient lighting and communications", Proc. SPIE 8282, Broadband Access Communication Technologies VI, vol. 8282, pp. 82820J-1-82820J-15, 2012.

[13] A. Jovicic, J. Li, and T. Richardson, "Visible Light Communication: Opportunities, Challenges and the Path to Market", IEEE Communications Magazine, vol. 51, no. 12, pp. 26-32, 2013.

[14] P. Louro et al., "Optical demultiplexer based on an a-SiC:H voltage controlled device", Phys. Status Solidi C, vol. 7, no. 3–4, pp. 1188–1191, 2010.

[15] P Louro, V Silva, I Rodrigues, M.A. Vieira, M Vieira "Transmission of Signals Using White LEDs for VLC Applications" - Materials Today: Proceedings, 3(3), 2016, pp. 780–787 doi:10.1016/j.matpr.2016.02.009.

[16] M. Vieira, M. A. Vieira, P. Louro, V. Silva, and P. Vieira, "Optical signal processing for indoor positioning using a-SiC:H technology", Opt. Eng., vol 55, no. 10, pp. 107105-1-107105-6, 2016.

[17] M. A. Vieira, M. Vieira, P. Louro, and P. Vieira, "Cooperative vehicular communication systems based on visible light communication," Opt. Eng., vol. 57, no. 7, pp. 076101, 2018.

[18] P. Louro, V. Silva, M. A. Vieira, and M. Vieira, "Viability of the use of an a-SiC:H multilayer device in a domestic VLC application", Phys. Status Solidi C, vol, 11, no. 11–12, pp. 1703–1706, 2014.

[19] P. Louro, J. Costa, M. Vieira, M. A. Vieira, and Y. Vygranenko, "Use of VLC for indoor navigation with RGB LEDs and a-SiC:H photodetector", Proc. of SPIE, Optical sensors, vol. 10231, pp. 102310F-1-102310F-10, 2017.

[20] P. Louro, J. Costa, M. A. Vieira, and M. Vieira, "Optical Communication Applications based on white LEDs", J. Luminescence, vol. 191, pp. 122-125, 2017.

[21] M. Vieira, M. A. Vieira, I. Rodrigues, V. Silva, and P. Louro, "Photonic Amorphous Pi'n/pin SiC Optical Filter Under Controlled Near UV Irradiation", Sensors & Transducers, vol. 184, no. 1, pp. 123-129, 2015.

[22] Y. Qiu, H.-H. Chen and W.-X. Meng, "Channel modeling for visible light communications—a survey", Wirel. Commun. Mob. Comput. 2016; 16:2016–2034, DOI: 10.1002/wcm.

[23] I. Raza, S. Jabeen, S. R. Chaudhry, S. Asad Hussain, "Optical Wireless Channel Characterization For Indoor Visible Light Communications", Indian Journal of Science and Technology, Vol 8 (22), DOI: 10.17485/ijst/2015/v8i22/70605, 2015.

[24] P. Louro, M. Vieira, M. A. Vieira, "Bidirectional visible light communication," Opt. Eng. 59(12), 127109 (2020), doi: 10.1117/1.OE.59.12.127109.

[25] P. Louro, M. Vieira, and M. A. Vieira "Indoor and outdoor geo-localization and navigation by visible light communication", Proc. SPIE 11713, Next-Generation Optical Communication: Components, Sub-Systems, and Systems X, 117130H (5 March 2021); https://doi.org/10.1117/12.2579342.

[26] M. A. Vieira, M. Vieira, P. Louro, L. Mateus, P. Vieira, "Indoor positioning system using a WDM device based on a-SiC: H technology", Journal of Luminescence 191, pp. 135-138.

[27] P. Louro, M. Vieira, M. A. Vieira, M. Fernandes and J. Costa (2011), "Use of a-SiC:H Photodiodes in Optical Communications Applications", Advances in Photodiodes, Gian Franco Dalla Betta (Ed.), ISBN: 978-953-307-163-3, InTech, Chap.19, pp:377-402 (2011).

[28] Datasheet with technical specifications: https://media.digikey.com/pdf/Data%20Sheets/CREE%20Power/CLV1A-FKB_Rev5.pdf, March 2020.

[29] Y. Zhu, W. Liang, J. Zhang, and Y. Zhang, "Space-Collaborative Constellation Designs for MIMO Indoor Visible Light Communications", IEEE Photonics Technology Letters, vol. 27, no. 15, pp. 1667–1670, 2015.

[30] S. I. Raza, et al., "Optical Wireless Channel Characterization For Indoor Visible Light Communications", Indian Journal of Science and Technology, vol. 8, no. 22, pp. 1 – 9, 2015.

[31] M.V. Bhalerao, M. Sumathi, and S.S. Sonavane, "Line of sight model for visible light communication using Lambertian radiation pattern of LED", International Journal of Communication Systems, 2016, https://doi.org/10.1002/dac.3250.

[32] M. A. Vieira, M. Vieira, P. Louro, V. Silva, A. S. Garção, "Photodetector with integrated optical thin film filters", Journal of Physics: Conference Series 421 (1), 012011.

A Cooperative and Coded Communication Scheme using Network Coding and Constructive Interference for Information-Centric Wireless Sensor Networks

Shintaro Mori
Department of Electronics Engineering and Computer Science
Fukuoka University
8-19-1 Nanakuma, Jonan-ku, Fukuoka 814-0180, Japan
e-mail: smori@fukuoka-u.ac.jp

***Abstract*—This paper presents a cooperative communication scheme for information-centric wireless networks, focusing on disaster-resilient smart-city applications. The proposed scheme uses a network coding technique and constructive interference to enhance data distribution and reduce radio interference between relay nodes. The results of computer simulations demonstrate the recoverability of forwarding data under the cross-interference environment and improvement in caching-data spread.**

Keywords-Information-centric wireless sensor networks; Network coding (NC); Cooperative communication

I. INTRODUCTION

Internet-of-things applications have become widespread across various domains, such as smart cities, industrial automation, healthcare, and "smart everything." This has been introduced to leverage Internet connectivity to turn objects into smart objects and enables devices to exchange information with each other and make decisions. For instance, smart-city applications can provide a solution for the issues resulting from urbanization, including social needs, and governmental structures [2]. These applications have led to an explosive increase in the number of edge-node devices. In other words, success in this context depends on the effective deployment of advanced wireless network technologies. In this occasion, machine-type communications, which are quite different from traditional human-type communications, must be investigated extensively. The features of these systems include low power, broad coverage, ultra-density, and mobile edge computing [3]. In addition, smart-city solutions face unique limitations due to unpredictable and non-uniform traffic, and some areas may be outside the wireless network coverage, such as rural areas or areas where a natural disaster has occurred [4]. Disaster-resilient smart cities require secure and reliable wireless communication because it is of extreme importance when dealing with users' health records and other sensitive information [5].

Various wireless communications and network protocols have been investigated to meet different requirements regarding the collection, distribution, security, and privacy of sensing data. Towards this end, wireless sensor networks (WSNs) have become an integral part of the future Internet framework to take advantage of various technologies across horizontal and vertical domains. One promising element of the solution for the above technique is the use of an information-centric network (ICN), (e.g., a content-centric network or named-data network). This next-generation network architecture is poised to replace the current IP-based networks [6]. It natively supports features, such as abstraction, naming, and in-network caching, which enables decoupling the data from its original location and adopting individual data-based security at the network-layer level. Therefore, the idea of ICN with WSNs is a suitable combination for the aforementioned background, which yields information-centric wireless sensor networks (ICWSNs).

ICWSNs implement a packet flooding (broadcasting) strategy, which generates numerous requesting packets, resulting in high traffic and network congestion. Although this paper does not focus on congestion control, it is essential to consider congestion when aiming to enhance ICWSNs. Therefore, it is imperative to develop a new ICN-based network protocol and friendly wireless communications technologies. However, to the best of our knowledge, suitable wireless systems have not yet been sufficiently investigated with respect to integrating communication, caching, computing, control, sensing, and localization technologies [7]. Such systems present several technical concerns, including limited battery power, range between devices, bandwidth, disconnectivity, network overload, data redundancy, communication overhead, network lifetime, lack of information, and data integration difficulties. As a medium access control (MAC) and physical layer (PHY) protocol underpinning ICWSNs, the ad-hoc wireless networking, and multi-hop relay networking techniques can be used as clues for practical usage. These technologies enhance the domain of autonomous-distributed services at the cost of efficient utilization of system resources [8].

We propose a cooperative communication scheme for underpinning effective ICWSN frameworks. The concept of cooperative communications can be used to increase the gains by harnessing the effects of path diversity, i.e., by having a relay node send the same data to a destination node if the data transmission is not successful. The proposed scheme uses a network coding (NC) [9] technique to minimize network traffic on relay nodes. However, NC-encoded packets generate an area of epidemic-packet collisions and congestion because the neighbor relay nodes forward the packets at the same time. Furthermore, in some cases, WSN devices simplify the protocol stacks, and omit synchronization and

collision avoidance mechanisms. The proposed scheme can reduce the radio interference among multiple relay nodes during the data flooding process by using constructive interference—if receiver-side nodes can detect a superposition of baseband signals from multiple transmitter-side nodes, the interference can be ignored [10].

The previous work [1] illustrated a blueprint of this study. On the other hand, the contributions of this paper are as follows: we propose a MAC/PHY protocol and evaluate the advantage of combining NC and constructive interference for the proposed scheme through fundamental PHY characteristics. We also evaluate the improvement to caching data deployment as a result of the proposed scheme.

The remainder of this paper is organized as follows. Section II presents an overview of the basic principle of cooperative communications. Section III introduces the proposed scheme, and Section IV presents the numerical results. Section V provides related work. Section VI concludes the paper with a brief summary and mention of future work.

II. COOPERATIVE COMMUNICATION TECHNOLOGIES

In this section, we introduce the key technologies, the NC technique and constructive interference that we use in the proposed scheme.

A. Network coding for cooperative communications

Communication between the source and destination takes place through different paths by means of cooperating entities called relays. Among the relay techniques in wireless (multi-hop and ad-hoc) networks, the decode-and-forward relaying method is used to decode the data that reaches the relay node and then re-encode and forward them. Another technique, the amplify-and-forward relaying method, can be selected as a simple forwarding mechanism. In the example shown in Figure 1, we focus on nodes $\mathbb{A}$, $\mathbb{B}$, and $\mathbb{C}$ and presume that $\mathbb{A}$ and $\mathbb{B}$ send $\mathbb{A}$'s data of $\boldsymbol{A}$ and $\mathbb{B}$'s data of $\boldsymbol{B}$, and $\mathbb{C}$ exchanges them as relay nodes. In this case, the data transmission is completed in four steps: sending $\boldsymbol{A}$ from $\mathbb{A}$ to $\mathbb{C}$, sending $\boldsymbol{B}$ from $\mathbb{B}$ to $\mathbb{C}$, forwarding $\boldsymbol{A}$ from $\mathbb{C}$ to $\mathbb{B}$, and forwarding $\boldsymbol{B}$ from $\mathbb{C}$ to $\mathbb{A}$. The NC technique is used here with the aim of improving throughput. When $\mathbb{C}$ transfers the bit-by-bit mixed data of $\boldsymbol{A}$ and $\boldsymbol{B}$ by utilizing an exclusive OR (XOR) operation, the data transmission procedure can be reduced to three steps: sending $\boldsymbol{A}$ from $\mathbb{A}$ to $\mathbb{C}$, sending $\boldsymbol{B}$ from $\mathbb{B}$ to $\mathbb{C}$, and forwarding $\boldsymbol{A} \oplus \boldsymbol{B}$ from $\mathbb{C}$ to $\mathbb{A}$ and $\mathbb{B}$ during broadcasting. After receiving $\boldsymbol{A} \oplus \boldsymbol{B}$, $\mathbb{A}$ can restore $\boldsymbol{B}$ by $(\boldsymbol{A} \oplus \boldsymbol{B}) \oplus \boldsymbol{A}$, and $\mathbb{B}$ can restore $\boldsymbol{A}$ in the same manner. Note that $\oplus$ denotes the XOR operator.

We note that if it is unnecessary for the relay node to know the exact source data, in other words, if the relay node does not need to cache the data, a physical-layer NC (PHY-NC) method can be adopted. In the PHY-NC method, the NC data is not decoded the individual data separately, and the combined signals are received simultaneously from two nodes into NC data. Therefore, general NC is introduced to decrease the number of required time slots to three, whereas PHY-NC can further reduce until two slots [11][12].

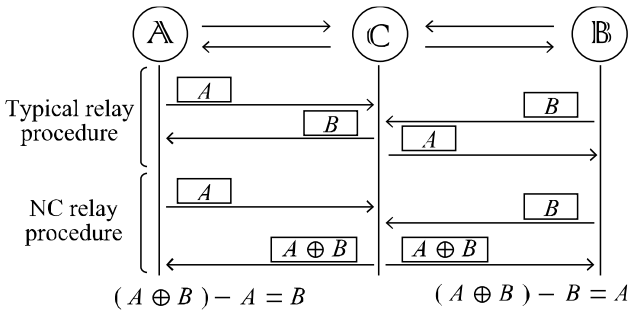

Figure 1. Network model of example node deployment for network coding technqiue in the proposed scheme

B. Constructive interference

Wireless communications cause interference whenever spatially close nodes transmit concurrently, namely, when they generate signals that overlap in time and space, and share the same radio frequency. Interference is generally disruptive and lowers the probability of successful packet reception. In contrast, when interference is constructive, if receiver-side nodes can detect a superposition of baseband signals from multiple transmitter-side nodes, the interference can be ignored. Namely, the superposition of several tolerable out-of-phase carrier signals enables correct detection with high probability. Constructive interference is especially useful when more than two nodes transmit concurrently. For instance, a flooding-based communication, such as in WSNs, is suitable and can propagate a packet for several (multi-hop) transmissions through the entire network without serious collisions.

III. PROPOSED SCHEME

ICN decouples the data from its original location using a name-based data-centric network scheme, which enables to cache and delivering the data regardless of the availability of the original (source) publisher. Moreover, ICN can provide content-based security, i.e., all security-sensitive information can be exchanged via the wireless channel. In this section, we provide an overview of the proposed scheme, including the proposed cooperative scheme, MAC protocol, and PHY protocol.

A. Proposed cooperative communications scheme

In-network caching—where each node duplicates the frequently used data by leveraging their embedded local (cache) storage—helps to decrease the end-to-end delay and reduce the network traffic. To accelerate the effect of in-network caching in ICWSNs, the nodes should actively accumulate the data as cached data. One of the key features of a wireless communication system is an overhearing phenomenon in which neighbor nodes can receive data whether or not it is desired. For example, in Figure 2(a), when $\mathbb{A}$ sends $\boldsymbol{A}$ to $\mathbb{C}$, $\mathbb{F}$, and $\mathbb{D}$ can also receive $\boldsymbol{A}$; likewise, when $\mathbb{B}$ sends $\boldsymbol{B}$ to $\mathbb{C}$, $\mathbb{G}$ can also receive $\boldsymbol{B}$. Therefore, the scheme achieves in-network caching for the nodes located along the

routing path (on-path caching) as well as those around the routing path (off-path caching).

For two-way network traffic, in other words, when the routing paths overlap in opposite directions, the NC technique can reduce the number of forwarded packets. In the relay phase, as shown in Figure 2(b), ℂ transmits $\boldsymbol{A} \oplus \boldsymbol{B}$ instead of $\boldsymbol{A}$ or $\boldsymbol{B}$. Here, due to the overhearing phenomena, $\boldsymbol{A} \oplus \boldsymbol{B}$ from ℂ can be received from 𝔸 and 𝔹 as well as from 𝔻 and 𝔼. Therefore, as the assist phase in the proposed scheme, as shown in Figure 2(b), 𝔻 and 𝔼 also send $\boldsymbol{A} \oplus \boldsymbol{B}$ as a helper with ℂ by performing multiplexing. As a result, if 𝔸 fails to receive $\boldsymbol{A} \oplus \boldsymbol{B}$ from ℂ, it can be recovered by utilizing $\boldsymbol{A} \oplus \boldsymbol{B}$ from 𝔻 due to the benefit of path diversity afforded through the different wireless channels. By using this mechanism, the nodes located around 𝔻 and 𝔼 but outside the coverage area of ℂ can be additionally off-path cached, which expands the number of new cashable nodes.

To support the cooperative mechanism, each node has three phases: transmit, relay, and assist. Every node regularly maintains standby (e.g., 𝔽 and 𝔾), and the status is changed to the transmit phase when the node makes a data transmission request (e.g., 𝔸 and 𝔹). While receiving surrounding (overheard) data, if the node receives two different data which should be forwarded, the status moves to the relay phase (e.g., ℂ). However, if the received data is NC-encoded data, the status switches to the assist phase (e.g., 𝔻 and 𝔼). The details of the proposed scheme's signal processing will be described in Section III.D.

B. Proposed MAC protocol

We assume the pure (unslotted) Aloha method is used as a channel access protocol in the MAC layer, which has been widely adopted as a channel access protocol in commercial low-power wide-area networks. An uncomplicated protocol is assumed to simplify the device implementation (including low-energy consumption), and because the synchronization among nodes is not practically available in ICWSNs. The current wireless communication systems using the pure-Aloha method presuppose that the data transmission has a sufficiently long interval, implying that collision or interference among nodes will not be fatal issues. However, as shown in Figure 3, in the proposed scheme, the relay nodes and assist nodes forward the NC-encoded data immediately (in the relay and assist phases), so collision and interference in a regional area are inevitable.

The proposed scheme utilizes constructive interference to tackle the issues regarding collision and interference caused by forwarding multiple NC-encoded packets. Namely, as shown in Figure 3, if the received NC-encoded packets (e.g., $\boldsymbol{A} \oplus \boldsymbol{B}$) are immediately forwarded in the assist phase, the interference of these packets (that are transmitted by 𝔻 and 𝔼) can be reduced. The primary reason that we assume an unsophisticated MAC protocol is to integrate the constructive interference effectively in the assist phase. In WSNs, constructive interference has not been extensively exploited because it is difficult to attain sufficiently accurate synchronization and highly predictable software delays are required. However, this approach is suitable for the scenarios in which the proposed scheme is applicable (i.e., in the relay and assist phases). Note that in cases where different data are in conflict with each other (destructive), the proposed scheme cannot be applied, which is beyond the scope of our present study.

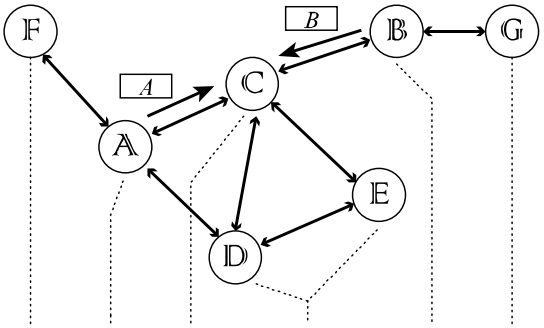

(a) Network model of example node deployment

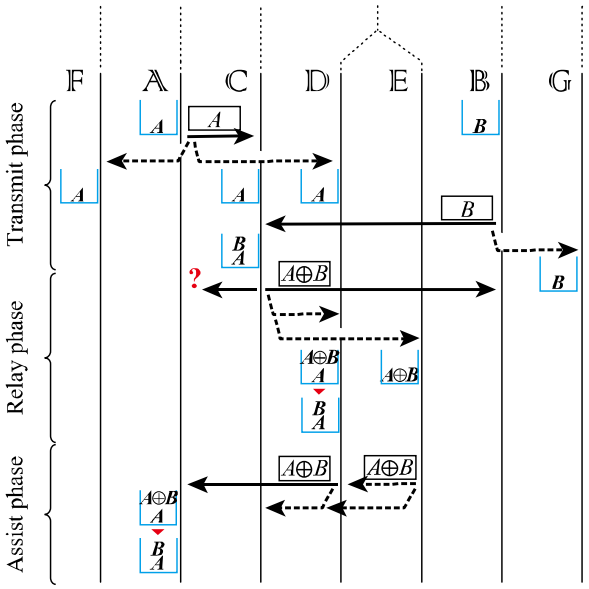

(b) Message and data flow of proposed data-forwarding processing

Figure 2. Proposed cooperative communication scheme

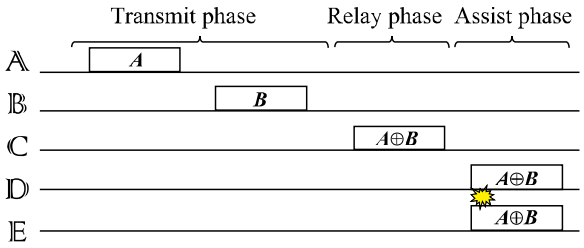

Figure 3. Baseline scenario of proposed scheme in MAC layer

C. Proposed PHY protocol

In the modulation scheme of digital wireless communication systems, $K\ (=\log_2 M)$ bits data are placed on the phase and/or amplitude of the transmitted waveform. Let T denote the time period required to transmit one symbol of the M -ary modulation method. In the baseband representation of the modulated waveform, a symbol $(s_{\mathrm{I}}, s_{\mathrm{Q}}) \in \mathbb{R}^2$ is defined as

$$\left(s_{\mathrm{I}}, s_{\mathrm{Q}}\right) \triangleq \left(s_{i_1}, s_{i_2}\right), (i = 1, 2, \cdots, M) \tag{1}$$

where $\mathbb{R}$ denotes the set of real numbers. A transmitted signal waveform, $s(t)(0 < t < T)$ is then represented by

$$s(t) = \Re(\ x(t)\ \mathrm{e}^{\mathrm{j}2\pi f_c t}\ ) \tag{2}$$

where the operator $\Re(\cdot)$ denotes real part, f_{c} denotes a radio-frequency (RF) carrier waveform, and $x(t) \triangleq \mathrm{s_I} + \mathrm{j}s_{\mathrm{Q}}$.

On the receiver side, if we ignore the effects of multipath fading and shadowing for simplicity, the wireless link is characterized as an additive Gaussian noise (AWGN) channel. Then, the received signal waveform $y_\ell(t)$ is expressed as

$$y_\ell(t) = s(t) + n_\ell(t) \tag{3}$$

where $n_\ell(t)$ is the AWGN, i.e., its (stochastic) random variable is depended on a normal distribution. During the relay and assist phases, the total signals received from the L nodes with a minute offset τ is given by

$$y(t) = \sum_{\ell=1}^{L} s(t)\ \delta(\mathrm{t} - \tau_\ell) + n_\ell(t) \tag{4}$$

where the operator $\delta(\cdot)$ means time shift by τ.

D. Signal processing of MAC and PHY protocols

The signal processing procedure of the proposed scheme is shown in Figure 4(a). The data frame corresponding to the sensing data is temporarily stored in the buffer memories and is pending until allowed to transmit from the transmission controller, along with the cooperative communications' data for the relay and assist phases. Figure 4(b) shows the states of the transmission controller: receive, transmit, relay, and assist. The transmit, relay, and assist states correspond to the three phases and append the receive state for standby. These states are switched depending on the state sequences (arrows between states) that are triggered by the radio events. When the node device needs to transmit the data, i.e., the data frame has arrived at the data buffer, the state is switched from receive to transmit, and then the data are sent. Similarly, while the node device is overhearing incoming data from the neighbors, when the NC-encoded data arrives, the state is switched from receive to assist. After data transmission is complete, it is switched back from the transmit or assist states to receive.

Meanwhile, the transmission controller periodically checks the status of neighbor nodes and has the database regarding the combination of relayed nodes, e.g., $\mathbb{C}$ should

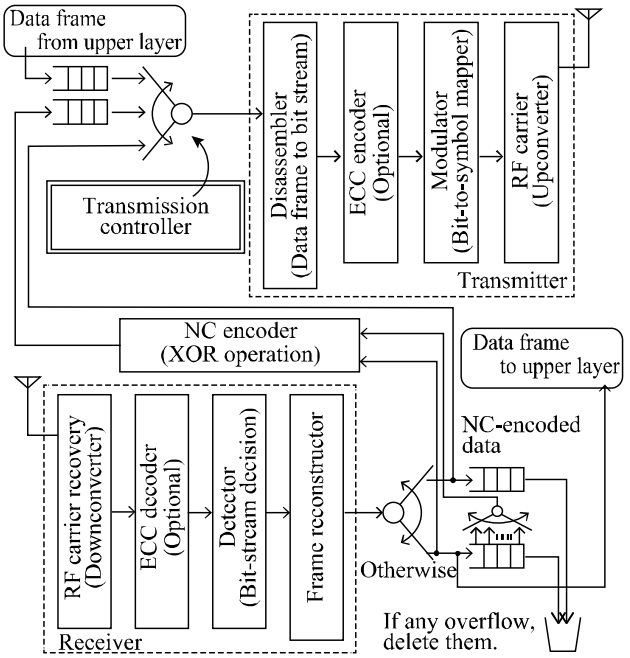

(a) Signal processing of the proposed scheme

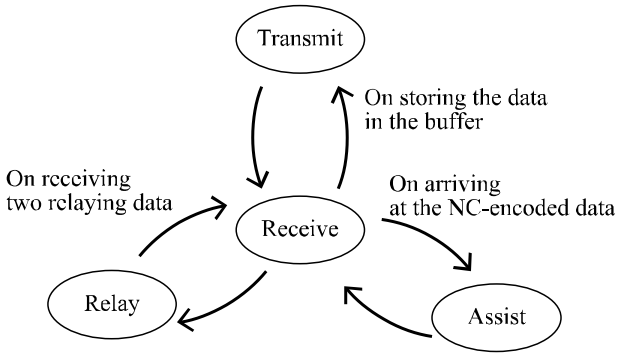

(b) State of the transmission-data controller

Figure 4. Signal processing of the proposed scheme

know $\mathbb{A}$ and $\mathbb{B}$ are the combinations of relayed nodes. Therefore, when the node device contains two data from the relayed nodes, it switches from receive to relay, and then it fulfills the relayed procedures. In this paper, we assume that every node knows whether it needs to relay the data, that the NC-encoded data's number of multi-hops is predefined, and that the nodes can determine their upper limitation of forwarding in order to avoid unlimited hops. Note that, if the node device is not in the receive state, it cannot switch between the transmit, assist, and relay states.

In the transmitter, as shown in Figure 4(a), the data frame is disassembled to the bit stream. Then the bit-based data are mapped into bit-to-symbols at the modulator (mapper) and superimposed on the RF carrier waveform to the antenna. In the receiver, the received signal is down-converted to the

baseband, demodulated, and detected, and then the recovered data are reconstructed to the data frame. The received data are classified as NC-encoded data or otherwise and respectively stored to data buffers. In addition, the error control coding (ECC) encoder and decoder are inserted between the frame (de)structure and (de)modulator if necessary. Unlike ordinal flooding mechanisms, the proposed scheme does not add any backoff, and the nodes transmit the same packet simultaneously immediately after the packet reception in the assist phase. By exploiting constructive interference phenomena, the proposed scheme can maintain a high packet reception rate despite allowing concurrent transmission. Therefore, if the received NC-encoded packets are forwarded immediately in the assist phase, the interference of packets transmitted will be reduced.

IV. COMPUTER SIMULATION

To evaluate the proposed scheme, we investigated the restorability of the baseband signal by using constructive interference and improvement in data caching among nodes.

A. Simulation environment for PHY performance

Assuming an experimental network composed of a relay node, an assist node, and a receiver node, we implemented a scenario in which the relay node and the assist node send the same data packet to the receiver node. In other words, it is the same as when $\mathbb{C}$ sends the NC-encoded data in the relay phase, $\mathbb{D}$ and $\mathbb{E}$ forward the data in the assist phase, and then $\mathbb{A}$ receives them (Figure 2). The computer simulation is conducted using the Matlab simulator. The waveforms of the radio signal arriving from the assist nodes are generated using the same data and system but with a time gap of τ.

The frame length was set as $1{,}000 \times \log_2 M$ bits, and the information bits were assigned by random values on the basis of the Bernoulli distribution with equal probability. Considering the wireless module to be installed in the WSN node device, the modulation scheme uses phase shift keying (PSK), in which the bits are superimposed on the phase of the carrier waveform. In particular, in (1), we consider M = 2, 4, and 8 for M-ary PSK methods, i.e., BPSK, QPSK, and 8-PSK, respectively. In addition, the bit-to-symbol mapping rule was used based on the optimum mapping pattern (Gray code). To minimize the complexity of the simulation and evaluate the fundamental performance of the proposed scheme, we ignore the fading and shadowing as in (3) due to SN mobility (i.e., assuming SNs are statically deployed and utilized). Namely, the channel is dominated by AWGN, and we assume that the number of assist nodes, L = 2 in (4), and their transmission power are the same parameters. We used a normalized signal-to-noise ratio (SNR) (that is, strictly SNR per bit or E_b/N_0) to represent the transmitted power in order to compare the performance of the different modulation schemes as a same condition.

B. Comparison of modulation methods

The simulation parameters are listed in Table I, and the result of bit error ratio (BER) performance of the different modulation methods are illustrated in Figure 5. The parameters are 1) type of modulation: BPSK, QPSK, and 8-

TABLE I. SIMULATION PARAMETERS

Terms	Values
Modulation method	BPSK, QPSK, 8PSK with Gray mapping rule
Frame length	1,000 bit (BPSK), 2,000 bit (QPSK), 3,000 bit (8PSK)
Error-control coding	N/A
Detector's decision type	Hard-decision
Sampling rate of waveform	16 samples/symbol
Channel model	AWGN channel

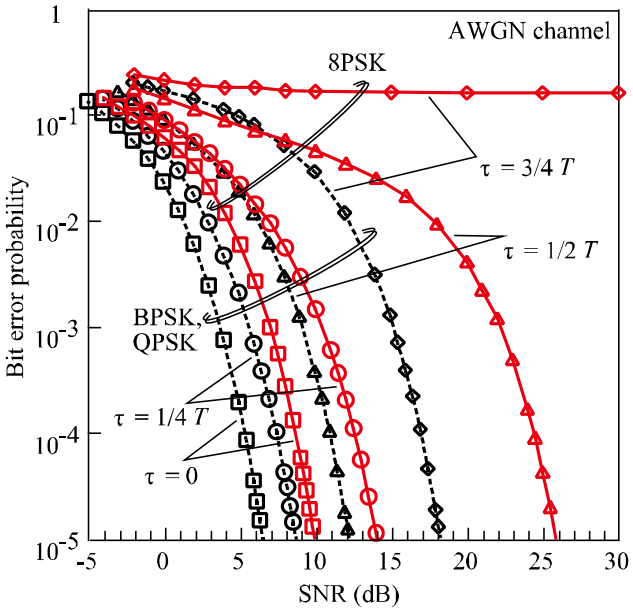

Figure 5. Bit error probability vs. SNR for BPSK, QPSK, and 8-PSK methods

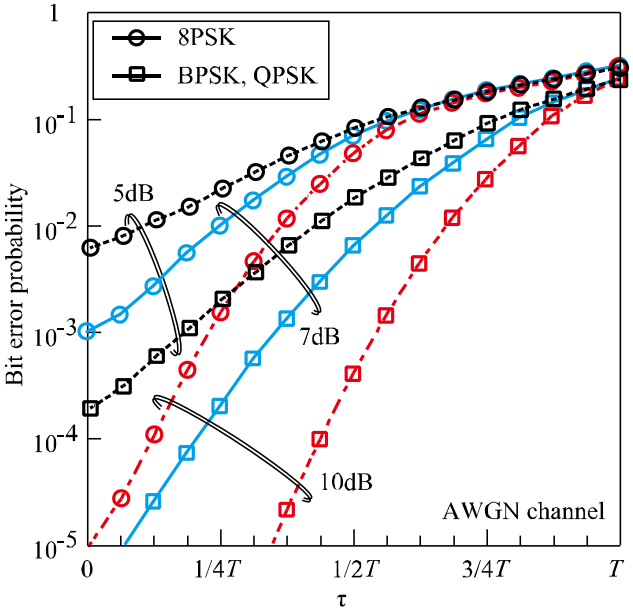

Figure 6. Bit error probability vs. time gap τ for BPSK, QPSK, and 8-PSK methods when SNRs were 5, 7, and 10 dB

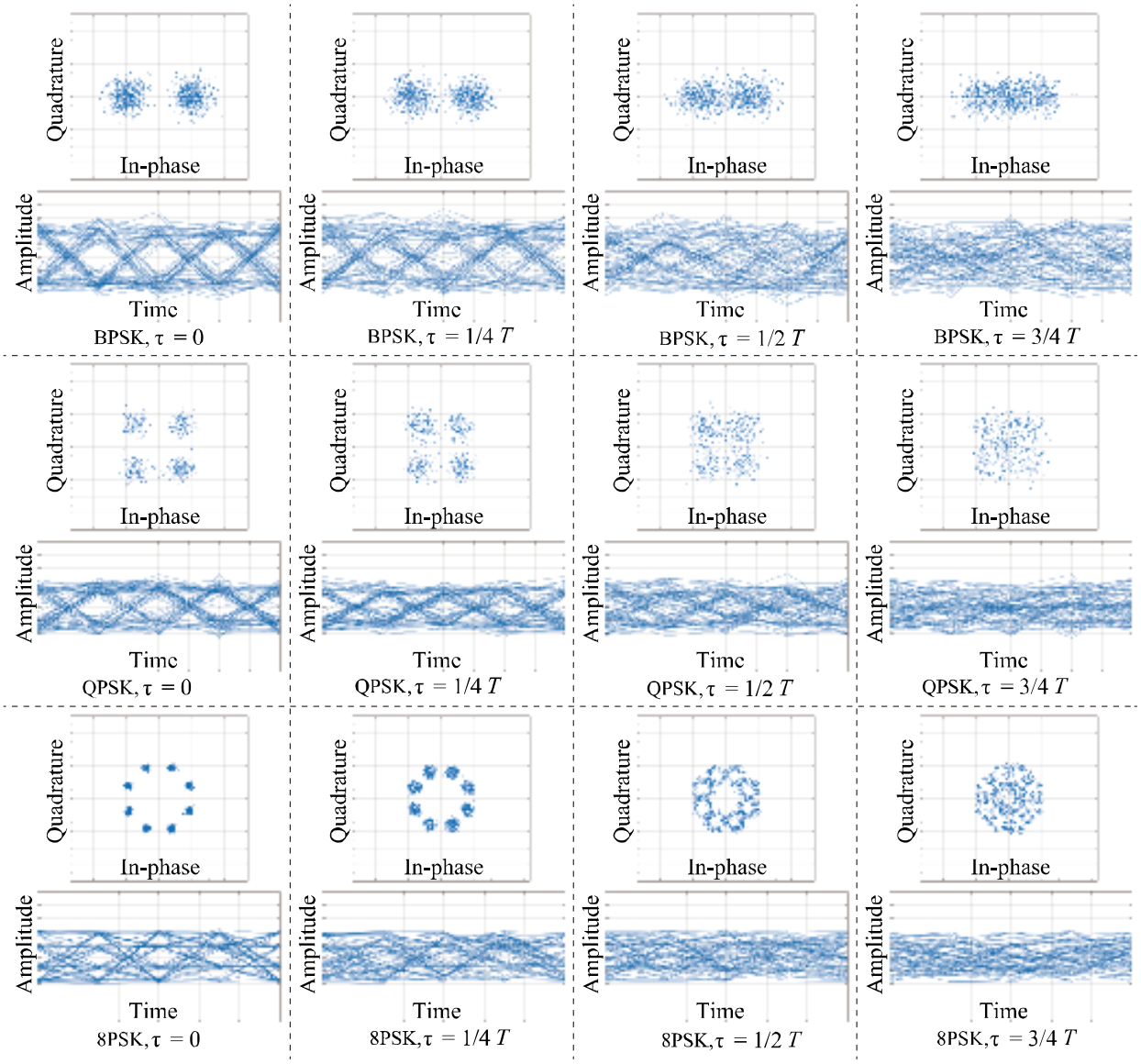

Figure 7. Perforamnce of teceiver-side detector, including constellation diagram and eye diagram, for received signals with a time lag.

PSK, 2) time gap: $\tau = 0$, (1/4) T, (1/2) T, and (3/4) T, and 3) SNR. The curves of BPSK and QPSK were overlapped (i.e., the result of BPSK and QPSK were the same) because their signal constellations (i.e., bit-to-symbol mapping pattern in (1)) are orthogonal. This indicates that the BPSK/QPSK methods are more effective than the 8-PSK method, and the major error mechanism is the time gap.

In the BPSK and QPSK methods, the SNR for 10^{-3} BER are 3.8 dB, 5.7 dB, 9.2 dB, 15.2 dB, and the SNR for 10^{-5} BER are 6.6 dB, 8.8 dB, 12.3 dB, and 18.3 dB for $\tau = 0$, (1/4) T, (1/2) T, and (3/4) T, respectively. In contrast, in the 8-PSK method, the SNR for 10^{-3} BER are 7.0 dB, 10.5 dB, and 22.2 dB, and the SNR for 10^{-5} BER are 10 dB, 14.1 dB, and 25.9 dB, respectively. In particular, the bit errors cannot be reducible (BER floor) in the case of 8-PSK with $\tau = (3/4)\ T$, even if the SNR is set as very large. Therefore, when the transmission data rate is higher (i.e., M is set as a large value), it is difficult to gain the effect of constructive interference. However, this is not a serious concern because the application service in which the proposed scheme will be deployed does not require high-speed and high-capacity wireless communications.

To investigate the effect of τ on the proposed scheme, in Figure 6, the results of the BER performance when τ is varied. The major parameters are considered as follows: 1) type of modulation: BPSK, QPSK, and 8-PSK, 2) SNR: 5 dB, 7 dB, and 10 dB, and τ. Increasing τ leads to a BER degradation, and the BER curve is not linear, i.e., the gradient of the BER curve becomes gradually relaxed, this means the effect on the

TABLE II. SIMULATION PARAMETERS

Terms	Values
Modulation method	BPSK with Gray mapping rule
Frame length	1,000 bit (BPSK)
Error-control coding	Uncoded, Convolutional coding with Viterbi decoding
Detector's decision type	Hard-decision
Sampling rate of waveform	16 samples/symbol
Channel model	Additive white Gaussian noise

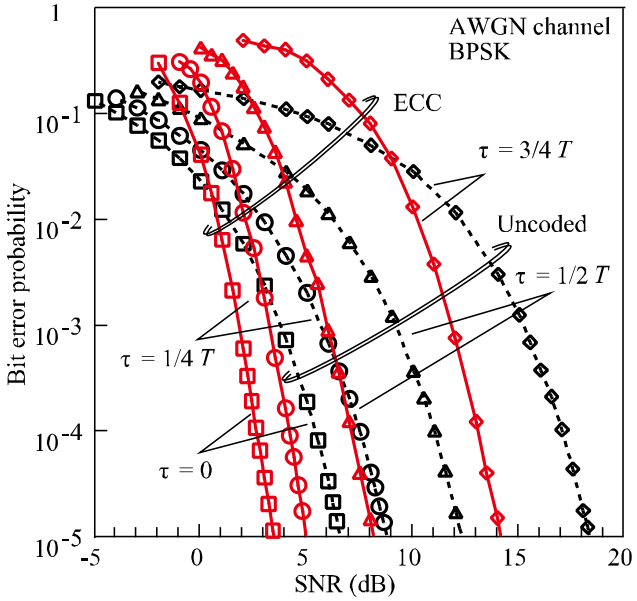

Figure 8. Bit error probability vs. SNR with and without ECC technique for BPSK method

BER should be significantly considered in the region where τ is as small as possible.

C. Received signal for detection

In the receiver, Figure 7 shows a received signal to be handled, i.e., the signal to be demodulated and detected. The parameters are 1) type of modulation: BPSK, QPSK, and 8-PSK, 2) time gap: τ = 0, (1/4) *T*, (1/2) *T*, and (3/4) *T*, 3) SNR set as 10 dB, and 4) the constellation and eye pattern (diagram) of the received signal. The results of the detector's performance indicate that the cases of τ = 0, (1/2) *T*, and (1/2) *T* had a clearly separated constellation of received signals and a clear eye pattern, while τ = (3/4) *T* had the opposite result and thus the detector could not decide (estimate) the transmitted data. This result is also well linked to the effects of τ on bit error probability, as shown in Figures 5 and 6.

D. Effect of error control coding scheme

In general, wireless communication systems mitigate packet errors using automatic repeat request and forward error correction. The former is out of scope in this paper because

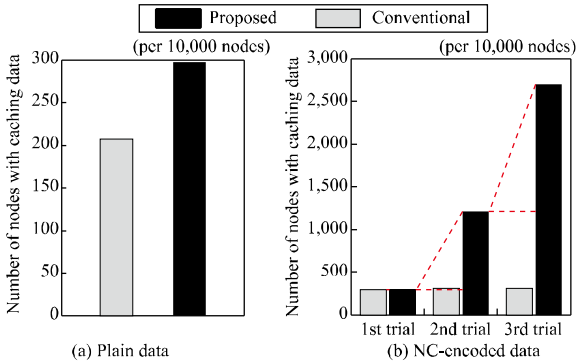

Figure 9. Number of successfully received nodes and cached data

we particularly focus on the relay and assist phases, while the latter is considered in this section. If a powerful ECC scheme is adopted, the processing delay will increase significantly. This leads to an increasing τ, which is detrimental to the proposed scheme. In addition, as the aforementioned results show, the BPSK method performs more noise resistance (in terms of bit error probability) than other methods, and it is commonly used in the node devices (i.e., that is supported as a basic modulation method) that consist of the application services in which the proposed scheme is deployed. Therefore, the simulation parameters are listed in Table II, and the results of bit error probability with and without the ECC method in the BPSK method are shown in Figure 8. The parameters are 1) type of modulation: BPSK, 2) type of ECC scheme: uncoded and convolutional code with Viterbi decoding scheme, 3) time gap: τ = 0, (1/4) *T*, (1/2) *T*, and (3/4) *T*, and 4) SNR.

The results illustrate that for τ = 0, (1/4) *T*, (1/2) *T*, and (3/4) *T*, thanks to introducing the ECC scheme, the SNR for 10^{-3} BER can improve by 2.0 dB, 2.5 dB, 3.2 dB, and 3.4 dB, and the SNR for 10^{-5} BER can improve by 3.2 dB, 3.8 dB, 4.1 dB, and 4.1 dB, respectively. Meanwhile, in the regions with small SNR (less than 0.5 dB, 1.7 dB, 3.8 dB, and 9.0 dB for τ = 0, (1/4) *T*, (1/2) *T*, and (3/4) *T*), BER performance with ECC cannot be improved; thus, there is no advantage to using the ECC scheme in these SNR regions.

E. Effectiveness of proposed scheme

To illustrate the benefit of the proposed scheme, we performed another evaluation using computer simulation implemented in C++ language. This simulation aims to illustrate that the proposed scheme can assist in maximizing the number of nodes with caching data. In the simulation, 10,000 nodes were deployed in a 1-km^2 area, the communication range of the nodes was set to 100 m, and the unreachable probability of the data (i.e., packet error ratio) was set to 5%. In the conventional scheme, the relay node forwards the NC-encoded data three times, whereas in the proposed scheme, the assist nodes that receive the NC-encoded data forward at the same time as the relay node. Because the assist nodes that receive the first-forwarded data from the relay station will transmit the data twice, and the nodes that receive the second-forwarded data will transmit them once. The end of the assist phase can align with the end

of the relay phase, and the proposed scheme can prevent infinite data flooding.

As seen in Figure 9(a), the number of successfully cached nodes per 10,000 was improved by 43.5% as a result of the assist nodes. For spreading the NC-encoded data, as shown in Figure 9(b), when the forwarding trials were increased, the nodes were enhanced by 306% and 123% for the proposed scheme compared to just 4.98% and 0.234% for the conventional scheme. At the end of the relay and assist phases, the proposed scheme could cache 8.61 times as many nodes as the conventional one. Note that to decode the NC-encoded data, plain data is required, e.g., either $\boldsymbol{A}$ or $\boldsymbol{B}$ for $\boldsymbol{A} \oplus \boldsymbol{B}$.

V. Related Work

The combination of NC and ICN has become a growing research interest. Montpetit et al. [13] utilized this combination in the internetworking layer by applying the NC technique to enhance the performance of data forwarding in ICNs. Mekbungwan et al. [14] proposed an NC-based data dissemination system made up of bulk data, such as photos, maps, and databases for situational awareness in post-disaster areas. Their system design was based on the store-carry-and-forward method in delay-torrent networking store-carry-and-forward method in order to reduce the amount of network traffic on relay nodes. For next-generation cellular networks, the packet duplication method is being introduced to meet the 99.999% reliability requirement, where the original packet and its duplicate are transmitted via two different physical paths, the concept of which is the same as the path-diversity technique [15]. However, the radio resource consumption is proportional to the number of data copies, and this duplication of data caching leads to a significant waste of radio resources. To tackle this problem, Zhu et al. [16] proposed a task-oriented communication method in which the waveform superposition property of a wireless channel is exploited to achieve over-the-air aggregation of data simultaneously transmitted by devices. The idea of overlaying signals can be seen as a kind of NC in the physical layer.

VI. Conclusion

We proposed a cooperative communication scheme using the NC technique with constructive interference for ICWSNs. The numerical results of our initial evaluation of the scheme indicated that a small gap of signals could be tolerated, and the proposed scheme could contribute to the distribution of cached data. In future work, because the recoverability of the received data depends on the signal gaps of the forwarded data, we should further investigate a technique that separates them. Moreover, we will expand the practical scenarios in which our scheme can be implemented to enhance the quality of service, lifetime, and robustness of the real smart-city site.

Acknowledgment

A part of this work was supported by JSPS KAKENHI Grant Number JP21H03436 and JP19K20261.

References

[1] S. Mori, "Cooperative communication scheme using network coding and constructive-interference phenomena for information-centric wireless networks," *Proc. IARIA the 21th Int. Conf. Networks (ICN 2022)*, Apr. 2021, pp. 1–4.

[2] N. Chen, T. Qiu, L. Zhao, X. Zhou, and H. Ning, "Edge intelligent networking optimization for Internet of things in smart city," *IEEE Wireless Commun.*, vol. 28, no. 2, pp. 26–31, Apr. 2021.

[3] F. Guo et al., "Enabling massive IoT toward 6G: A comprehensive survey," *IEEE Internet of Things J.*, vol. 8, no. 15, pp. 11891–11915, Aug. 2021.

[4] M. El-Tanab and W. Hamouda, "An overview of uplink access techniques in machine-type communications," *IEEE Network*, vol. 35, no. 3, pp. 246–251, May/June 2021.

[5] Y. Li, Y. Yu, W. Susilo, Z. Hong, and M. Guizani, "Security and privacy for edge intelligence in 5G and beyond networks: Challenges and solutions," *IEEE Wireless Commun.*, vol. 28, no. 2, pp. 63–69, Apr. 2021.

[6] O. Serhane, K. Yahyaoui, B. Nour, and H. Moungla, "A survey of ICN: Content naming and in-network caching in 5G and beyond networks," *IEEE Internet of Things J.*, vol. 8, no. 6, pp. 4081–4104, Mar. 2021.

[7] B. Ji et al., "Several key technologies for 6G: Challenges and opportunities," *IEEE Commun. Std. Mag.*, vol. 5, no. 2, pp. 44–51, June 2021.

[8] O. Hayat, Z. Kaleem, M. Zafarullah, R. Ngah, and S. Z. M. Hashim, "Signaling overhead reduction techniques in device-to-device communications: Paradigm for 5G and beyond," *IEEE Access*, vol. 9, pp. 11037–11050, 2021.

[9] D. Umehara, T. Hirano, S. Denno, M. Morikura, and T. Sugiyama, "Wireless network coding in slotted aloha with two-hop unbalanced traffic," *IEEE J. Sel. Areas in Commun.*, vol. 27, no. 5, pp. 647–661, June 2009.

[10] F. Ferrari, M. Zimmerling, L. Thiele, and O. Saukh, "Efficient network flooding and time synchronization with Glossy," *Proc. ACM/IEEE Int. Conf. Info. Process. Sensor Networks (IPSN)*, Apr. 2011, pp. 73–84.

[11] S. Zhang, S. C. Liew, and L. Lu, "Physical layer network coding schemes over finite and infinite fields," *Proc. IEEE Global Telecommun. Conf. (GLOBECOM)*, Dec. 2008, pp. 1–6, doi: 10.1109/GLOCOM.2008.ECP.726.

[12] P. Mach and Z. Becvar, "Device-to-device relaying: Optimization, performance perspectives, and open challenges towards 6G networks," *IEEE Commun. Surveys & Tutorials*, vol. 24, no. 3, pp. 1336–1393, thirdquarter 2022.

[13] M. Montpetit, C. Westphal, and D. Trossen, "Network coding meets information-centric networking: An architectural case for information dispersion through native network coding," *Proc. ACM WS Emerging Name-Oriented Mobile Networking Design-Architecture, Algorithms, and App. (NOM)*, June 2012, pp. 31–36, doi: 10.1145/2248361.2248370.

[14] P. Mekbungwan, A. Tunpan, and K. Kanchanasut, "An NC-DTN framework for many-to-many bulk data dissemination in OLSR MANET," *Proc. Int. Wireless Commun. and Mobile Comp. Conf. (IWCMC)*, Aug. 2015, pp. 964–969, doi: 10.1109/IWCMC.2015.7289213.

[15] S. Baek, D. Kim, M. Tesanovic, and A. Agiwal, "3GPP new radio release 16: Evolution of 5G for industrial Internet of things," *IEEE Commun. Mag.*, vol. 59, no. 1, pp. 41–47, Jan. 2021.

[16] G. Zhu, J. Xu, K. Huang, and S. Cui, "Over-the-air computing for wireless data aggregation in massive IoT," *IEEE Wireless Commun.*, vol. 28, no. 4, pp. 57–65, Aug. 2021.